

The compositional variability of eudialyte-group minerals

J. SCHILLING¹, F.-Y. WU², C. McCAMMON³, T. WENZEL¹, M. A. W. MARKS¹, K. PFAFF¹, D. E. JACOB⁴ AND G. MARKL^{1,*}

¹ Mathematisch-Naturwissenschaftliche Fakultät, Fachbereich Geowissenschaften, Universität Tübingen, Wilhelmstraße 56, D-72074 Tübingen, Germany

² State Key Laboratory of Lithospheric Evolution, Institute of Geology and Geophysics, Chinese Academy of Sciences, P.O. Box 9825, Beijing 100029, China

³ Bayerisches Geoinstitut, Universität Bayreuth, Universitätsstraße 30, D-95447 Bayreuth, Germany

⁴ Institut für Geowissenschaften und Earth System Science Research Centre, Johannes Gutenberg-Universität, JJ. Becher-Weg 21, D-55128 Mainz, Germany

[Received 6 October 2010; Accepted 24 January 2011]

ABSTRACT

Eudialyte-group minerals (EGM) represent the most important index minerals of perodic agpaitic systems. Results are presented here of a combined EPMA, Mössbauer spectroscopy and LA-ICP-MS study and EGM which crystallized in various fractionation stages from different parental melts and mineral assemblages in silica over- and undersaturated systems are compared. Compositional variability is closely related to texture, allowing for reconstruction of locally acting magmatic to hydrothermal processes. Early-magmatic EGM are invariably dominated by Fe whereas hydrothermal EGM can be virtually Fe-free and form pure Mn end-members. Hence the Mn/Fe ratio is the most suitable fractionation indicator, although crystal chemistry effects and co-crystallizing phases play a secondary role in the incorporation of Fe and Mn into EGM. Mössbauer spectroscopy of EGM from three selected occurrences indicates the $\text{Fe}^{3+}/\Sigma\text{Fe}$ ratio to be governed by the hydration state of EGM rather than by the oxygen fugacity of the coexisting melt. Negative Eu anomalies are restricted to EGM that crystallized from alkali basaltic parental melts while EGM from nephelinitic parental melts invariably lack negative Eu anomalies. Even after extensive differentiation intervals, EGM reflect properties of their respective parental melts and the fractionation of plagioclase and other minerals such as Fe-Ti oxides, amphibole and sulphides.

KEYWORDS: eudialyte group minerals, crystal chemistry, agpaitic systems.

Introduction

EUDIALYTE, first described by Stromeyer (1819) from the Ilímaussaq intrusive complex (South Greenland), encompasses a group of Na-Ca-Zr silicates of trigonal symmetry with 22 independent mineral species (Rastsvetaeva, 2007). The IMA-accepted formula (Johnsen *et al.*, 2003) for the eudialyte group is $N_{15}[M(1)]_6[M(2)]_3[M(3)][M(4)]Z_3[\text{Si}_{24}\text{O}_{72}]O'_4X_2$ with

$N = \text{Na, Ca, K, Sr, REE, Ba, Mn, H}_3\text{O}^+$;

$M(1) = \text{Ca, Mn, REE, Na, Sr, Fe};$
 $M(2) = \text{Fe, Mn, Na, Zr, Ta, Ti, K, Ba, H}_3\text{O}^+;$
 $M(3, 4) = \text{Si, Nb, Ti, W, Na};$
 $Z = \text{Zr, Ti, Nb};$
 $O' = \text{O, OH}^-, \text{H}_2\text{O};$
 $X = \text{H}_2\text{O, Cl}^-, \text{F}^-, \text{OH}^-, \text{CO}_3^{2-}, \text{SO}_4^{2-}, \text{SiO}_4^{4-}.$

Eudialyte-group minerals (EGM) are characteristic minerals of some highly evolved, peralkaline [molar $(\text{Na}+\text{K})/\text{Al} > 1$] mantle-derived magmatic rocks (e.g. Sørensen, 1974, 1992, 1997; Kogarko *et al.*, 1982, 2010). In syenitic systems, EGM are typomorphic minerals of so-called agpaitic rocks, in which High Field Strength Elements (HFSE; such as Zr, Hf, Nb, Ta, REE, Y) are incorporated into complex K-Ca-Na-silicates such as EGM (Sørensen, 1992, 1997; Marks *et al.*, 2011). They

* E-mail: markl@uni-tuebingen.de
DOI: 10.1180/minmag.2011.075.1.87

TABLE 1. Summary of the characteristics of the EGM investigated and background on the occurrences. Accessory minerals are not listed.

Locality	Geological frame and apparent parental melt composition of EGM-bearing unit(s)	Major co-existing Fe-Mg silicates and felsic minerals	Occurrence and petrography of EGM	Observed zoning patterns of EGM	Interpreted crystallization stage of EGM
Himaussaq, S Greenland	Proterozoic complex in the failed rift Gardar province ^{1,2,3} , alkali basaltic parental melt ⁴	Cpx, Amp ^{1,5,6,7,8,9} Afs, Nph, Sdl, Ab ^{1,5,6,7,8,9}	Major phase in various foid syenites ¹ in primary magmatic layering ^{2,5,6} ; in pegmatites ^{8,9} ; euhedral–subhedral (Fig. 1a,b) ^{1,6} , locally porphyritic or interstitial EGM crystals ⁸	Locally primary magmatic complex sector and oscillatory zonations ^{6,8,9}	Early- to late-magmatic
Mont Saint-Hilaire, SE Canada	Cretaceous complex of the Monteregian Hills province ^{10,11,12,13,14,15,16} , alkali basaltic parental melt ^{14,15}	Cpx, ±Amp, ±AGM ^{10,11} Afs, Nph, ±Sdl, ±Zeo, Ab ^{10,11}	Minor phase in various foid syenites ^{0,11} , in pegmatites, vugs and cavities ^{0,11} ; euhedral–anhedral, interstitial, locally porphyritic, aggregate-forming EGM crystals in vugs and cavities (Fig. 1e,f) ^{10,11}	Primary magmatic complex sector and oscillatory zonations; secondary zoning and replacement textures	Late- to post-magmatic
Ascension, Central Atlantic	Quaternary OIB ¹⁷ ; alkali basaltic parental melt ¹⁸	Cpx ¹⁷ Afs, Qz ¹⁷	Minor phase in peralkaline granite ^{17,18} ; invariably interstitial EGM crystals (Fig. 1g) ¹⁷	None	Late-magmatic
Straumsvola, Antarctic	Sub-intrusion of the Jurassic Karoo LIP ^{19,20,21} ; alkali basaltic parental melt ²¹	Cpx ²⁰ Afs, Nph or Qz ²⁰	Minor interstitial, porphyritic crystals in granite ²⁰ ; cm-sized anhedral minor late-stage EGM crystals in foid syenite ²⁰	Primary sector zoning patterns	Late-magmatic
Langsund archipelago, S Norway	Palaeozoic intrusive complex of the Oslo rift system ^{22,23} ; alkali basaltic parental melt ²³	Cpx ²²⁻²⁴ Afs, Nph ^{22,24}	Constituent in pegmatites of foid syenite ^{22,24,25,26}	None	Late-magmatic
Khibiny, NW Russia	Complex in the Devonian Kola Peninsula failed rift ^{27,28,29} ; nephelinitic parental melt ³⁰	Cpx, ±Amp, ±AGM ³⁰ Afs, Nph, ±Sdl ³⁰	Major and minor phase in various foid syenites and related pegmatites (Fig. 1c) ^{31,32} ; euhedral–anhedral, locally aggregate-forming EGM crystals of variable size ²⁴	Primary sector and oscillatory zoning patterns	Early- to late-magmatic
Lovozero, NW Russia	Complex in the Devonian Kola Peninsula failed rift ^{27,28,29} ; nephelinitic parental melt ³⁰	Cpx ³¹ Afs, Nph, Sdl ³¹	Major and minor phase in pegmatites of various foid syenites (Fig. 1d) ³² ; Euherdral-anhedral EGM of variable size ²⁴	Primary sector and oscillatory zoning patterns	Late-magmatic ³²

Tamazeght, Morocco	Isolated Eocene complex in the High Atlas Mountains ^{33,34,35,36,37} , nephelinitic parental melt ^{35,36,37}	Cpx ^{34,35} AfS, Nph, ±Sdl ^{34,35}	Minor-major constituent in pegmatites and veins of foid syenite ^{33,34} , euhedral–subhedral EGM crystals of variable size ³⁴	Late- to post-magmatic
Poços de Caldas, SE Brazil	Cretaceous complex; rift-related ^{38,39} , nephelinitic parental melt ^{38,39}	Cpx ^{38,24} Nph ^{38,24}	Minor constituent in late-stage environments of foid syenites ³⁸ , subhedral, poikilitic aggregates of EGM	Late-magmatic
Saima, N China	Triassic complex, rift-related ²⁴ ; nephelinitic parental melt	Cpx ²⁴ Nph ²⁴	Minor late-stage phase; constituent in layered foid syenites ²⁴ ; euhedral EGM crystals of variable size	Late-magmatic
Pilansberg, RSA	Mesoproterozoic poly-phase complex ^{40,41} ; unknown parental melt composition	Cpx, AGM, ±Amp ⁴² Nph, Sdl, ±Zeo ⁴²	Major constituent of late-magmatic to hydrothermal assemblages in foid syenites ^{42,43} , anhedral, poikilitic EGM crystals of variable size, strongly altered ^{42,43}	Late- to post-magmatic
Kipava, SE Canada	Proterozoic complex, Quebec Grenville province ^{44,45} ; metamorphic overprint	Amp Agrillite ⁴⁵	Locally important phase in metamorphosed foid syenites ^{44,45} , locally aggregates of cm-sized EGM crystals ⁴⁶	Late-magmatic
Norra Kärr, S Sweden	Isolated Proterozoic intrusive body ^{46,47} ; Metamorphic overprint	Amp, ±Cat ^{46,48} Nph ^{46,48}	Minor phase in schistose foid syenite (Fig. 1 <i>h</i>) ^{46,47,48} , euhedral-poikilitic EGM crystals (Fig. 1 <i>h</i>)	Late-magmatic

¹Markl *et al.* (2001); ²Ussing (1912); ³Ferguson (1964); ⁴Marks *et al.* (2004a); ⁵Bohse *et al.* (2001); ⁶Pfaff *et al.* (2008); ⁷Bailey *et al.* (2001); ⁸Schollenbruch (2007); ⁹Hettmann (2009); ¹⁰Horváth and Gault (1990); ¹¹Wight and Chao (1995); ¹²Adams (1903); ¹³Gold (1967); ¹⁴Eby (1985); ¹⁵Greenwood and Edgar (1984); ¹⁶Currie *et al.* (1986); ¹⁷Harris *et al.* (1982); ¹⁸Roedder and Coombs (1967); ¹⁹Harris (1986); ²⁰Harris and Rickard (1987); ²¹Leat *et al.* (2007); ²²Larsen (2010); ²³Anthony *et al.* (1989); ²⁴Wu *et al.* (2010); ²⁵Brogger, 1890); ²⁶Andersen *et al.* (2010); ²⁷Gerasimovskiy *et al.* (1974); ²⁸Sørensen (1997); ²⁹Sørensen (1990); ³⁰Kramm and Kogarko (1994); ³¹Kogarko *et al.* (1982); ³²Arzamastsev *et al.* (2002); ³³Shand (2002); ³⁴Shand (1990); ³⁵Shand (1998); ³⁶Schilling *et al.* (2009); ³⁷Shand (2008a); ³⁸Boutabdi *et al.* (1998); ³⁹Lastrino *et al.* (2003); ⁴⁰Williams-Jones (1999); ⁴¹Williams-Jones (1999); ⁴²Edgar and Blackburn (1972); ⁴³Olivo and Williams-Jones (1999); ⁴⁴Allan (1992); ⁴⁵Edgar and Blackburn (2006); ⁴⁶Törnebohm (1906); ⁴⁷Blackland (1977); ⁴⁸Adamson (1944).

also occur rarely in peralkaline granites (e.g. Harris and Rickard, 1987; Harris *et al.*, 1982).

EGM are generally found in various intraplate settings and may crystallize during different fractionation stages (Table 1; Kogarko *et al.*, 1982; Sørensen, 1997). For example, at the type locality, Ilímaussaq (S Greenland), EGM are orthomagmatic (Fig. 1a,b) as well as late magmatic (e.g. Bohse *et al.*, 1971; Pfaff *et al.*, 2008; Hettmann, 2009) and are associated locally with albite and analcime in late-stage veins (Schollenbruch, 2007). Similarly, the large alkaline complexes of the Kola Peninsula (Khibiny and Lovozero, NW Russia; Fig. 1c,d) have crystallized EGM from early- to late-magmatic stages (e.g. Kogarko *et al.*, 1982; Arzamastsev *et al.*, 2002). In other occurrences, EGM are restricted to late- to post-magmatic stages, such as in Mont Saint-Hilaire (Horváth and Gault, 1990; Fig. 1e,f) the Pilansberg complex (Mitchell and Liferovich, 2006), in the Langesund archipelago, S Norway (Andersen *et al.*, 2010; Larsen, 2010), or in the Tamazeght complex, Morocco (Schilling *et al.*, 2009). In rare cases, EGM are found in metamorphic rocks, such as in Norra Kärr, S Sweden (Adamson, 1944; Blaxland, 1977; Fig. 1g) and Kipawa, Quebec, Canada (Allan, 1992).

Typical minerals associated with EGM (Table 1) include aegirine and arfvedsonite, various Na-Al-silicates such as alkali feldspar, nepheline, sodalite, locally occurring zeolites, and a large number of rare HFSE- and Large Ion Lithophile Elements (LILE; such as Li, B, Be, Na, Sr)-incorporating minerals, such as astrophyllite- and lamprophyllite-group minerals, tugtupite and minerals of the wöhlerite, rosenbuschite and rinkite groups (e.g. Sørensen, 1997; Andersen *et al.*, 2010; Marks *et al.*, 2011). In rare granites, EGM coexist with quartz (Harris and Rickard, 1987; Harris *et al.*, 1982; Fig. 1h).

Some peralkaline rocks and especially EGM-bearing perodic agpaites are spatially and

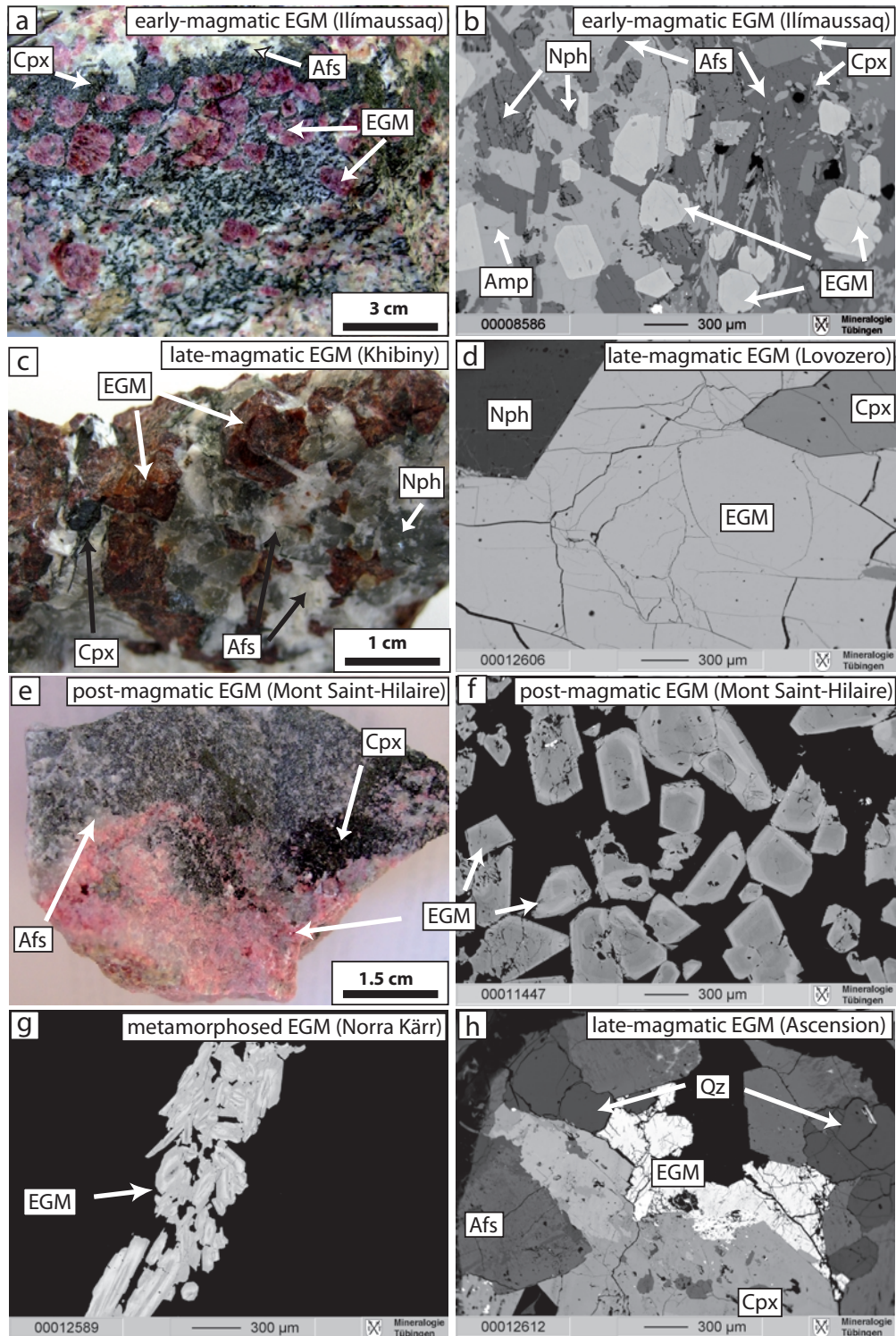
temporally related to some of most reduced igneous rocks (see Markl *et al.*, 2010, and references therein), and less fractionated rock units predating the agpaitic stage indicate relatively reduced but variable conditions below the FMQ buffer in different complexes (e.g. Ilímaussaq: $\Delta\text{FMQ} = -2$ to -5 , Marks and Markl, 2001; Motzfeldt: $\Delta\text{FMQ} = -0.5$ to -2 , Schönenberger and Markl, 2008; Tamazeght: $\Delta\text{FMQ} \approx -2$, Marks *et al.*, 2008a; Mont Saint-Hilaire: $\Delta\text{FMQ} \approx -1$, Schilling *et al.*, 2011). However, the lack of pertinent thermodynamic data and late-stage resetting effects make it impossible to directly constrain the oxygen fugacity in agpaites (e.g. Marks *et al.*, 2008a; Schönenberger and Markl, 2008).

A few recent studies showed that the combination of texture, assemblage and mineral chemistry of EGM can be a valuable indicator for a variety of magmatic to hydrothermal processes. For example, Pfaff *et al.* (2008) used compositional changes in EGM from the layered nepheline syenites at Ilímaussaq to infer replenishment and degassing processes of an agpaitic magma chamber. Coulson and Chambers (1996) and Coulson (1997) reconstructed the interaction of subsequently intruding melt batches using EGM textures. In a similar manner, Mitchell and Liferovich (2006) used three late- to post-magmatic EGM generations to reconstruct pH changes in the late-stage agpaitic Pilansberg system and Schilling *et al.* (2009) combined textural and compositional variations of EGM to decipher the interaction of agpaites with carbonatitic fluids in the Tamazeght Complex, Morocco. Since the work of Wu *et al.* (2010), it is clear that EGM can be used for U-Pb age determination, which adds a new dimension to its petrological applications.

As shown by Mitchell and Liferovich (2006) and Schilling *et al.* (2009), the highly variable composition of EGM may be used to decipher

FIG. 1 (facing page). Photomicrographs and BSE images of EGM-textures: (a) hand specimen showing early-magmatic EGM in layered kakortokite from the Ilímaussaq intrusion; (b) BSE image of early-magmatic EGM from a kakortokite sample of Ilímaussaq; (c) pegmatite hand specimen from Khibiny consisting of coarse-grained EGM, nepheline, aegirine and alkali feldspar; (d) BSE image of unzoned EGM in pegmatite from Lovozero; (e) hand specimen with post-magmatic EGM from a cavity in syenites from Mont Saint-Hilaire; (f) BSE image of EGM from the same sample as e showing post-magmatic EGM to be euhedral and primary oscillatory zoned; (g) zoned EGM in schistose rock from Norra Kärr; (h) BSE image of EGM associated with quartz in granite from Ascension Island. Afs = alkali feldspar, Amp = amphibole, Cpx = clinopyroxene, Nph = nepheline, Qz = quartz. See Schilling *et al.* (2009) and Wu *et al.* (2010) for more textures from other occurrences.

COMPOSITIONAL VARIABILITY OF EUDIALYTE-GROUP MINERALS



compositional and/or physico-chemical changes in evolving magmatic and hydrothermal systems. To explore the suitability of this mineral group for inferring petrological information, we investigated an extensive suite of EGM from different localities using electron probe micro-analysis (EPMA), laser ablation inductively coupled plasma mass spectroscopy (LA-ICP-MS) and Mössbauer spectroscopy. The main sample set includes EGM from Ilímaussaq, Tamazeght and Mont Saint-Hilaire, for which details on the petrology such as f_{O_2} estimates and the mineral assemblages in which EGM occur are available. The selection of this suite of samples covers all textural varieties of EGM (euclihedral early-magmatic to interstitial late-magmatic varieties, examples from pegmatites and post-magmatic hydrothermal veins; Fig. 1) and three magmatic systems that crystallized under markedly different f_{O_2} conditions. In addition to this suite of samples, we compare EGM from other feldspathoid- and quartz bearing rocks and metamorphic occurrences. Hence, we group our analyses based on (1) the stage during which EGM crystallized (i.e. on a textural basis, we distinguish early-, late- and post-magmatic and metamorphic EGM); (2) the mineral assemblages of major rock-forming phases; (3) the apparent composition of the parental melt; and (4) SiO_2 -saturation (i.e. feldspathoid- vs. quartz-bearing systems). Furthermore, we compare $Fe^{3+}/\Sigma Fe$ Mössbauer spectroscopic data of EGM from Ilímaussaq, Tamazeght and Mont Saint-Hilaire and check for interrelations between $Fe^{3+}/\Sigma Fe$ in EGM and the redox states of rocks from these three complexes.

We emphasize that the aim of the present paper is not to treat crystallographic aspects, nor to put further constraints on possible site occupancies of the EGM structure. Instead our results place constraints on similarities and differences in the evolution of peralkaline EGM-crystallizing melts. Table 1 summarizes relevant petrographic characteristics such as co-existing minerals, textural position and zoning patterns of the EGM investigated, and describes the host rocks of the EGM-bearing assemblages.

Methods

Electron probe micro-analyses

Most electron probe micro-analyses (EPMA) of EGM were performed using a JEOL 8900 electron microprobe at the University of Tübingen,

Germany. To avoid volatilization, we analysed Na first and checked for stability of the signal over the Na counting time. We used identical analytical conditions to those described by Pfaff *et al.* (2010) and Schilling *et al.* (2009) except for the beam size, which we varied between 10 and 20 μm depending on the EGM grain size. Samples described by Wu *et al.* (2010) were analysed by the method described in their work and EGM from Pilansberg were analysed using the conditions given by Mitchell and Liferovich (2006; see the electronic supplement, deposited with the editor and available from http://www.minersoc.org/pages/e_journals/dep_mat_mm.html). Formulae of EGM were calculated on the basis of $(Si+Zr+Ti+Nb+Al+Hf) = 29$ a.p.f.u. (Johnsen and Grice, 1999).

Laser Ablation Inductively Coupled Plasma Mass Spectrometry (ICP-MS)

Trace elements were analysed either using the methods described by Wu *et al.* (2010) or *in situ* with an Agilent 7500ce Quadrupole ICP-MS coupled to a New Wave Research Merchantek UP-213 laser unit (Nd:YAG laser, output wavelength 213 nm) at the University of Mainz, Germany, following the procedure of Jacob (2006). Helium was used as the carrier gas and material was ablated with variable spot sizes between 55 and 100 μm . Average pulse energies varied between 0.2 and 0.3 mJ/pulse and pulse frequencies of 5 Hz were used for analyses on thin sections and 10 Hz for analyses of EGM embedded in epoxy disks. Each analysis consisted of 60 s background measurement followed by 60 s ablation time (10 ms per peak and isotope). ^{28}Si was used as an internal standard with Si concentrations determined by EPMA. The NIST SRM 612 glass served as an external standard and USGS BCR2-G was analysed as an unknown using Si concentrations listed in the GeoReM (<http://georem.mpch-mainz.gwdg.de/>) database (cf. Jochum and Nohl, 2008). For data processing we used the commercial GLITTER software (version 4.4.2; Macquarie University; Griffin *et al.*, 2008). Detection limits (DL) for most trace elements are <0.1 ppm, except for B, Ti, Cr, and Zn where the DL is <1 ppm. Phosphorus has a detection limit of ~ 2 ppm. Accuracy (1σ) based on the analyses of the BCR standard, which was analysed at least every 15 analyses, is within $\pm 10\%$ for most elements (including the REE) and ± 11 , 25 and 33% for B, P and Zn, respectively (see Appendix).

Mössbauer spectroscopy

Room-temperature spectra were recorded in transmission mode on a constant acceleration Mössbauer spectrometer with a nominal 370 MBq ^{57}Co high specific activity source (active area 500 $\mu\text{m} \times 500 \mu\text{m}$) in a 12 μm thick Rh matrix. The velocity scale was calibrated relative to 25 μm -thick α -Fe foil using the positions certified for (former) National Bureau of Standards standard reference material no. 1541; line widths of 0.36 mm/s for the outer lines of α -Fe were obtained at room temperature. Aggregates of 600–1500 μm length/width and 300–500 μm thickness from three selected EGM were analysed (effective Mössbauer thickness 3.7–5 mg Fe/cm²). The sample pieces were mounted on mylar film using colourless nail varnish and then centred over a hole drilled in a 25 μm thick Ta foil (absorbs 99% of 14.4 keV gamma rays). Each spectrum was collected over 1 day and fitted using the commercially available fitting program NORMOS written by R.A. Brand (distributed by Wissenschaftliche Elektronik GmbH, Germany).

Results

Major and minor elements

For the present study, we performed almost 1350 electron microprobe analyses of EGM in 123 samples from 13 localities (Fig. 2). We ensured that the complete compositional range of EGM was covered by carefully analysing all heterogeneities visible in BSE images. Typical analyses of EGM from all occurrences are presented in Table 2; the full range of analyses is provided in the electronic supplement, deposited with the editor and available at http://www.minersoc.org/pages/e_journals/dep_mat_mm.html.

Figure 2a shows the compositional ranges of Fe, Mn, Sr and the variable Si contents that add to 24 tetrahedrally coordinated Si forming the Si-rings of the EGM structure. Fe and Mn correlate negatively in EGM from all occurrences but concentration levels are not necessarily identical, as exemplified by EGM from Ilímaussaq, Mont Saint-Hilaire and Tamazeght (Fig. 2b). Ilímaussaq (including analyses from Schollenbruch, 2007; Pfaff *et al.*, 2008; Hettmann, 2009) has crystallized Fe-rich EGM; whereas Mn-dominant EGM formed at Tamazeght and Mont Saint-Hilaire. Manganese and Fe, among other cations, can occupy more than one structural site in the structural formula

(Johnsen *et al.*, 2003) and Fe, in particular, may be present in various oxidation states (Pol'shin *et al.*, 1991; Khomyakov *et al.*, 2010). Vacancies can be present on some crystallographic sites and overall charge balance can be achieved by variably charged H-bearing species (H_3O^+ , OH^- , H_2O). These features render it effectively impossible to determine correct exchange vectors, but at least on the scale of a single intrusive complex, Mn/Fe systematically increases with texturally later-formed EGM and secondary zonation patterns.

Together, EGM from Ilímaussaq, Tamazeght and Mont Saint-Hilaire represent most of the Fe-Mn-Sr composition space observed with EGM from all occurrences investigated (Fig. 3). Strontium contents in EGM are highly variable and in all EGM from Ilímaussaq and Mont Saint-Hilaire (among other occurrences, such as Ascension, Straumsvola and Langesund; Figs 2a, 3), Sr does not correlate with textural changes or variable mineralogy. However, the greatest Sr contents are found in late-stage EGM from Pilansberg and Tamazeght (Mitchell and Liferovich, 2006; Schilling *et al.*, 2009). EGM from metamorphosed complexes and quartz-bearing assemblages plot close to the Fe-Mn tie line and do not show distinct enrichment of Sr.

In terms of the distribution of Na, Ca and Sr, most EGM from Ilímaussaq, Tamazeght and Mont Saint-Hilaire are relatively rich in Na; whereas EGM from some other occurrences (represented by the grey field) are Ca- and/or Sr-rich (Fig. 3b). Nb is enriched to stronger degrees than Ti in all EGM (Fig. 3c). Again, EGM from Ilímaussaq, Tamazeght and Mont Saint-Hilaire represent most of the composition space and metamorphosed and EGM coexisting with quartz are compositionally indistinguishable from such EGM that are not metamorphosed or that coexist with feldspathoids (Fig. 3). Table 3 summarizes minimum and maximum values (i.e. the overall range) of most elements analysed and molar Mn/Fe ratios.

In general, EGM from quartz-bearing rocks do not contain more Si than EGM from SiO_2 -undersaturated occurrences, and EGM from granitic rocks from Straumsvola are slightly lower in Si than those of nepheline syenitic rocks from the same locality (Fig. 2a). Some analyses show Si to be >26 a.p.f.u. (the sum of 24 tetrahedrally coordinated Si plus Si on the $M(3)$ and $M(4)$ sites), indicating that Si may occupy other structural sites.

TABLE 2. Typical EPMA analyses of EGM from the various occurrences.

Wt.%	Ilm GM1369_06	Ilm GM1335_20	Ilm ILM101_04	MSH MSH52_EGM1	MSH MSH52_EGM3	MSH MSHLVMA5_EGM1	MSH MSHT612_EGM4	Asc H30(1)29	Sr ST34_EGM2	Sr ST38neu_EGM1	Sr ST38neu_EGM1	Lgs LGS 02
SiO ₂	54.82	52.02	52.84	47.73	48.82	48.00	51.39	48.37	51.49	45.73	45.73	50.20
TiO ₂	0.03	0.01	b.d.l.	0.02	0.01	0.06	0.19	0.33	0.12	0.17	0.17	0.10
ZrO ₂	12.89	12.73	12.74	9.91	10.52	11.60	10.23	11.26	10.53	9.03	12.00	n.a.
HfO ₂	n.a.	n.a.	n.a.	0.26	0.21	0.17	0.14	0.30	0.25	0.21	n.a.	n.a.
Al ₂ O ₃	n.a.	n.a.	n.a.	0.04	0.05	0.22	0.10	0.02	0.19	b.d.l.	n.a.	n.a.
Nb ₂ O ₅	0.09	b.d.l.	b.d.l.	3.11	2.10	2.01	1.09	1.09	0.90	3.70	1.90	3.70
La ₂ O ₃	0.47	0.45	0.45	2.11	1.15	2.48	0.21	0.89	0.20	2.22	0.81	2.22
Ce ₂ O ₃	1.03	0.99	0.89	3.37	1.61	5.09	0.34	2.08	0.44	4.13	4.13	4.13
Nd ₂ O ₃	0.20	0.28	0.31	0.58	0.27	1.42	0.05	0.90	0.11	1.20	1.20	b.d.l.
Y ₂ O ₃	n.a.	n.a.	n.a.	0.45	0.36	1.01	b.d.l.	4.11	0.14	1.12	n.a.	n.a.
FeO	4.02	6.58	6.44	5.20	5.93	2.38	3.13	5.23	6.35	6.66	6.04	6.04
MnO	1.19	0.61	0.99	4.02	2.37	3.82	2.81	2.05	1.26	8.82	3.19	3.19
CaO	11.15	10.81	10.40	8.12	10.32	3.43	10.08	4.01	10.92	5.31	11.71	11.71
SrO	b.d.l.	b.d.l.	b.d.l.	b.d.l.	b.d.l.	b.d.l.	b.d.l.	b.d.l.	0.23	0.11	b.d.l.	b.d.l.
Na ₂ O	12.63	14.36	13.41	13.50	14.05	16.46	16.42	13.84	14.59	13.00	11.49	11.49
K ₂ O	n.a.	n.a.	n.a.	0.32	0.36	0.29	0.40	0.56	0.42	0.21	n.a.	n.a.
Cl	1.13	1.18	1.05	1.03	1.48	0.75	0.66	1.98	1.37	0.71	0.71	0.71
O=Cl	0.26	0.27	0.24	0.23	0.33	0.17	0.15	0.45	0.31	0.16	0.16	0.16
Total	99.39	99.76	99.27	99.54	99.28	99.00	97.37	96.56	99.19	96.17	99.00	99.00
Formula based on Σ (Si Zr Ti Nb Al Hf) normalized to 29 a.p.f.u.												
Si	25.99	25.91	25.95	25.58	25.73	25.35	26.07	25.64	26.01	25.51	25.51	25.51
Ti	0.01	0.00	0.01	0.00	0.02	0.07	0.13	0.05	0.05	0.07	0.04	0.04
Zr	2.98	3.09	3.05	2.59	2.70	2.99	2.53	2.91	2.59	2.46	2.46	2.46
Hf	n.a.	n.a.	n.a.	0.04	0.03	0.03	0.02	0.04	0.04	0.03	n.a.	n.a.
Al	n.a.	n.a.	n.a.	0.03	0.03	0.13	0.06	0.01	0.11	b.d.l.	n.a.	n.a.
Nb	0.02	b.d.l.	b.d.l.	0.75	0.50	0.48	0.25	0.26	0.21	0.93	0.44	0.44
La	0.08	0.08	0.08	0.42	0.22	0.48	0.04	0.17	0.04	0.46	0.15	0.15
Ce	0.18	0.18	0.18	0.66	0.31	0.98	0.06	0.40	0.08	0.84	0.19	0.19
Nd	0.03	0.05	0.05	0.11	0.05	0.27	0.01	0.17	0.02	0.24	b.d.l.	b.d.l.
Y	n.a.	n.a.	n.a.	0.13	0.10	0.28	b.d.l.	1.16	0.04	0.33	n.a.	n.a.
Fe ²⁺	1.59	2.74	2.65	2.33	2.61	1.05	1.33	2.32	2.68	0.31	2.57	2.57
Mn ²⁺	0.48	0.26	0.41	1.83	1.06	1.71	1.21	0.92	0.54	4.17	1.38	1.38
Ca	5.67	5.77	4.66	5.83	1.94	5.48	2.28	5.91	3.17	6.38	6.38	6.38
Sr	b.d.l.	b.d.l.	b.d.l.	b.d.l.	b.d.l.	b.d.l.	0.08	0.07	0.07	0.04	b.d.l.	b.d.l.
Na	11.61	13.87	12.77	14.03	14.36	16.85	16.15	14.22	14.29	14.06	11.34	11.34
K	n.a.	n.a.	n.a.	0.22	0.24	0.20	0.26	0.38	0.27	0.15	n.a.	n.a.
Cl	0.91	1.00	0.87	0.94	1.32	0.67	0.57	1.78	1.17	0.67	0.61	0.61

Wt.%	Khib 392-0_EGM2	Khib KB-1 05	L _{ov} LV02 07	L _{ov} 364_EGM2	PDC PDC 06	PDC PDC 06	Sm SM2.06	K _{PW} KPW 04	NK NK_EGM1
SiO ₂	50.78	51.30	52.18	49.57	54.57	57.13	52.26	52.44	
TiO ₂	0.24	0.57	0.49	0.54	0.50	0.25	0.24	0.14	
ZrO ₂	10.22	12.94	12.34	13.06	12.26	13.59	11.91	10.73	
HfO ₂	0.23	n.a.	n.a.	0.29	n.a.	n.a.	n.a.	0.21	
Al ₂ O ₃	0.10	n.a.	n.a.	0.26	n.a.	n.a.	n.a.	0.14	
Nb ₂ O ₅	1.59	b.d.l.	0.54	0.21	0.21	1.19	0.50	0.09	
La ₂ O ₃	0.72	0.06	0.33	0.30	0.19	0.61	0.33	0.08	
Ce ₂ O ₃	0.96	0.11	0.67	0.63	0.22	0.94	0.66	0.24	
Nd ₂ O ₃	0.13	b.d.l.	0.17	0.31	b.d.l.	0.09	0.18	0.08	
Y ₂ O ₃	0.20	n.a.	n.a.	0.46	n.a.	n.a.	n.a.	0.74	
FeO	2.24	5.43	4.77	4.67	3.34	3.42	2.50	5.18	
MnO	4.14	0.36	1.84	1.83	4.22	2.61	1.39	1.36	
CaO	9.19	11.31	10.14	6.59	11.02	7.61	13.24	10.05	
SrO	1.42	0.75	b.d.l.	0.61	0.99	2.16	b.d.l.	b.d.l.	
Na ₂ O	12.01	14.48	15.68	16.70	11.03	9.11	14.28	13.03	
K ₂ O	0.35	n.a.	n.a.	0.39	n.a.	n.a.	n.a.	0.24	
Cl	1.15	1.27	0.69	1.11	0.77	0.64	0.56	0.38	
O=Cl	0.26	0.29	0.16	0.25	0.17	0.14	0.13	0.09	
Total	95.42	98.27	99.14	97.62	99.15	99.18	96.68	96.31	
Formula based on Σ (Si Zr Nb Al Hf) normalized to 29 a.p.f.u.									
Si	25.90	25.63	25.84	25.23	25.93	25.69	25.92	26.20	
Ti	0.09	0.21	0.18	0.21	0.18	0.08	0.09	0.05	
Zr	2.54	3.15	2.98	3.24	2.84	2.98	2.88	2.61	
Hf	0.03	n.a.	n.a.	0.04	n.a.	n.a.	n.a.	0.03	
Al	0.06	n.a.	n.a.	0.16	n.a.	n.a.	n.a.	0.08	
Nb	0.37	b.d.l.	b.d.l.	0.12	0.05	0.24	0.11	0.02	
La	0.14	0.01	0.06	0.06	0.03	0.10	0.06	0.02	
Ce	0.18	0.02	0.12	0.12	0.04	0.16	0.12	0.04	
Nd	0.02	b.d.l.	0.03	0.06	b.d.l.	0.01	0.03	0.01	
Y	0.05	n.a.	n.a.	0.12	n.a.	n.a.	n.a.	0.20	
Fe ²⁺	0.96	2.27	1.98	1.99	1.33	1.29	1.04	2.16	
Mn ²⁺	1.79	0.15	0.77	0.79	1.70	0.99	0.58	0.58	
Ca	5.02	6.05	5.38	3.59	5.67	7.03	5.38		
Sr	0.42	0.22	b.d.l.	0.18	0.27	0.56	b.d.l.		
Na	11.88	14.03	15.05	16.48	10.17	7.95	12.53	13.83	
K	0.23	n.a.	n.a.	n.a.	n.a.	n.a.	n.a.	0.15	
Cl	0.99	1.07	0.58	0.96	0.62	0.48	0.47	0.33	

n.a. = not analysed; b.d.l. = below detection limit; Ilm = Ilmaussaq, MSH = Mont Saint-Hilaire, Asc = Ascension, Str = Straumsvola, Lgs = Langesund, Khib = Khibiny, Lov = Lovozero, PDC = Poços de Caldas, Sm = Saima, Kpw = Kipawa, NK = Norra Kärr.

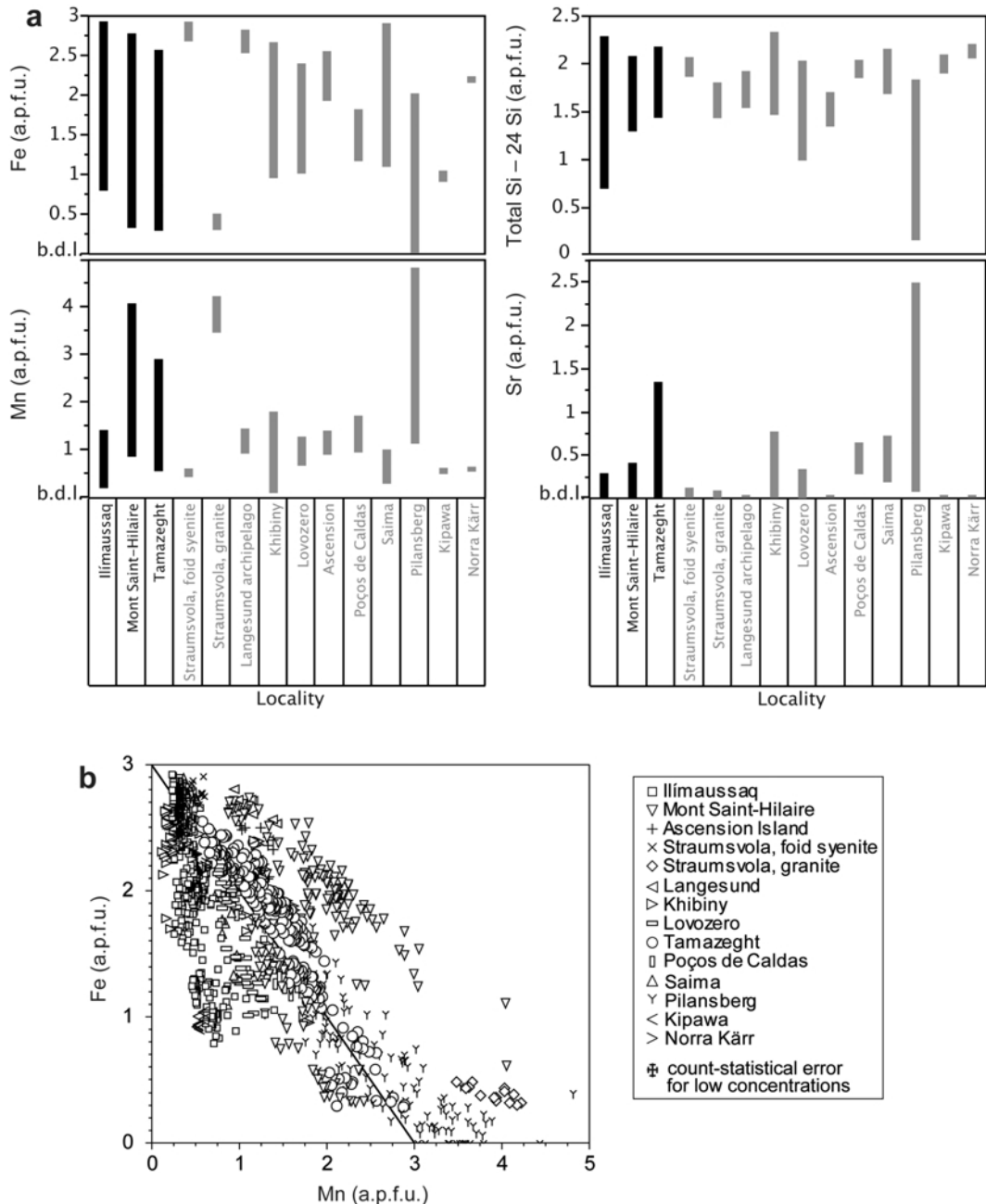


FIG. 2. (a) Variation of Fe, Mn, total Si-24 Si related to the ring structure, and Sr in EGM from all occurrences investigated. Element concentrations are given in a.p.f.u. (b) Mn vs. Fe (a.p.f.u.) for EGM from all occurrences investigated. Number of analyses: Ilímaussaq: 603, Mont Saint-Hilaire: 174, Tamazeght: 210, Straumsvola (foid syenite): 16, Straumsvola (granite): 14, Langesund: 8, Khibiny: 81, Lovozero: 43, Ascension: 23, Poços de Caldas: 8, Saima: 22, Pilansberg: 128, Kipawa: 8, Norra Kärr: 4.

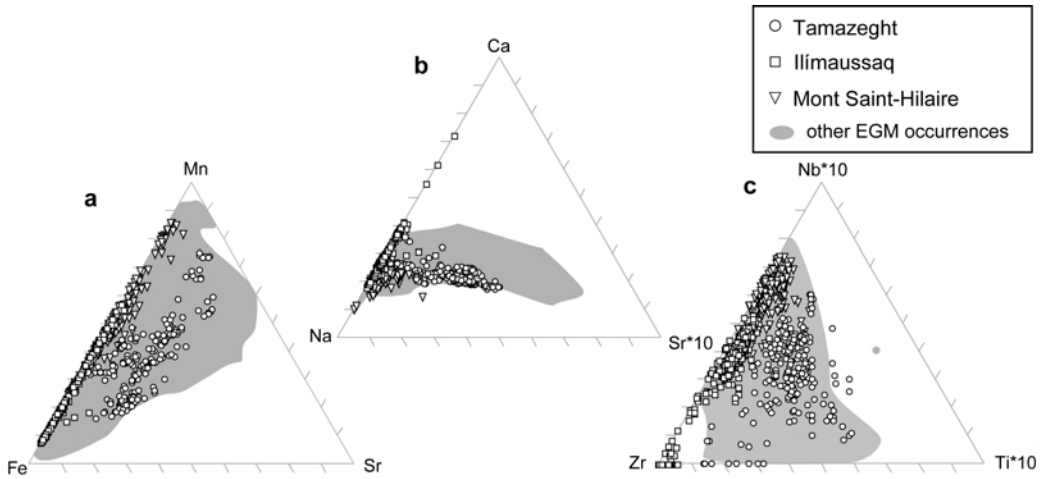


FIG. 3. Ternary diagrams showing compositional variation of EGM in the systems Fe-Mn-Sr, Na-Ca-Sr and Zr-Ti-Nb (a.p.f.u.).

Iron valence and site distribution

Mössbauer spectra of EGM collected from Ilímaussaq, Mont Saint-Hilaire and Tamazeght resemble those reported in the literature (Pol'shin *et al.*, 1991; Khomyakov *et al.*, 2010) and were fitted according to the model of Khomyakov *et al.* (2010) to quadrupole doublets with conventional constraints (component linewidths and areas assumed to be equal), where a maximum of three quadrupole doublets was sufficient to account for all absorption (Fig. 4). Centre shift and quadrupole splitting values of the subspectra fall within the ranges for the particular iron species reported by Khomyakov *et al.* (2010), enabling a robust assignment of valence and site coordination (a full list of hyperfine parameters of the fitted spectra are given in Table 2 of the electronic supplement). The relative areas can be taken to a first approximation to represent the relative abundance of the different iron species. The iron in all samples occurs predominantly as

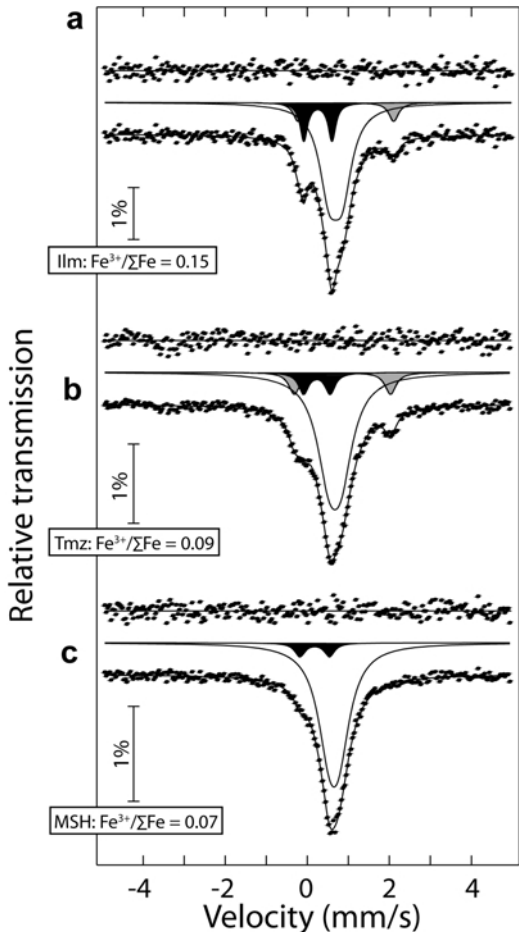


FIG. 4 (right). Room-temperature Mössbauer spectra of EGM. (a) Ilímaussaq (ILM101); (b) Tamazeght (TMZ177); (c) Mont Saint-Hilaire (MSHT613). Doublets are shaded as follows: black ($V^3\text{Fe}^{3+}$ and/or $V^3\text{Fe}^{3+}$); grey ($V^2\text{Fe}^{2+}$); unshaded ($IV\text{Fe}^{2+}$). Residuals above each spectrum indicate the difference between experimental and calculated data points, and the relative areas of each subspectrum indicate roughly the relative abundance of the particular species.

TABLE 3. Summary of concentrations of major and minor elements and element ratios of EGM from the various localities investigated.

§	*	Range Fe			Range Mn			Range Na			Range Ca			Range Sr			Range Si			Range Nb			Range Ti			Range Zr			Range Cl			Range Mn/Fe (molar)			Range U/Th			Range Nb/Ta			Range Zr/Hf		
		(ap.f.u.)																																									
Ilimaussaq	603	67	0.79–2.93	0.21–1.4	2.11–18.11	3.22–6.14	b.d.l.–0.27	24.7–26.28	b.d.l.–0.33	b.d.l.–0.07	2–3.14	0.19–1.76	0.08–1.32	0.5–3.1	7.8–22.3	0.01–4.4	4.8–99.7	37.1–72.9	33.4–97.6	Mont Saint-Hilaire	174	74	2.75–2.93	0.87–4.05	12.65–17.43	1.94–5.92	b.d.l.–0.41	25.31–26.07	0.21–0.86	b.d.l.–0.18	2.43–2.99	0.3–1.36	0.32–7.09	0.01–4.4	4.8–99.7	33.4–97.6							
Ascension	23	2	1.94–2.52	0.92–1.4	13.76–16.31	1.72–2.34	b.d.l.	25.36–25.69	0.26–0.57	0.13–0.27	2.61–2.95	1.65–1.86	0.4–0.71	0.1–0.2	14.4–22.5	1.1–1.4	6.5–7.9	43.4–50.9	46.6–49.7	Straunsvola (fooid-syenite)	16	6	2.68–2.91	0.44–0.6	13.78–15.93	5.91–6.65	0.03–0.1	25.88–26.06	0.21–0.3	0.05–0.07	2.52–2.64	1.17–1.35	0.15–0.22	1.1–1.4	6.5–7.9	43.4–50.9	46.6–49.7						
Straunsvola (granite)	14	2	0.31–0.49	3.48–4.22	13.4–14.58	2.79–3.42	b.d.l.–0.07	25.45–25.8	0.55–0.95	0.06–0.1	2.46–2.58	0.56–0.78	7.18–13.49	2.9–5.8	9.9–14	46.7–48.7	46.7–48.7	Langeund archipelago	8	8	2.53–2.81	0.94–1.42	11.05–11.86	6.36–6.65	b.d.l.	25.55–25.91	0.12–0.44	b.d.l.–0.05	2.88–3.04	0.53–0.61	0.33–0.56	0.1–0.1	14.3–15.4	24.1–25.2	24.1–25.2								
Khibiny	81	81	0.96–2.66	0.1–1.79	9.53–15.66	4.87–6.84	b.d.l.–0.76	25.47–26.33	b.d.l.–0.45	0.04–0.43	2.36–3.25	0.57–1.71	0.04–1.87	0.02–3.6	6.2–35.7	45.3–74.7	45.3–74.7	Lovezero	43	43	1.01–2.38	0.68–1.27	13.03–17.57	3.32–5.44	b.d.l.–0.32	25–26.03	b.d.l.–0.15	0.12–0.35	2.81–3.62	0.52–1.01	0.3–1.12	0.5–2.2	7.7–15	42.6–60.9	42.6–60.9								
Tamazeghit	210	31	0.29–2.56	0.57–2.88	7.84–15.55	4.45–6.8	b.d.l.–1.33	25.44–26.17	b.d.l.–0.7	0.04–0.43	2.42–3.28	0.11–1.36	0.22–1.04	0.1–3.6	79.6–338.2	62.5–128.8	62.5–128.8	Poços de Caldas	10	10	1.17–1.81	0.96–1.72	8.46–11.78	5.48–5.71	0.27–0.63	25.86–26.03	0.04–0.2	0.18–0.21	2.7–2.84	0.62–0.78	0.53–1.35	1.3–2.1	35.9–57.5	53.7–65.2	53.7–65.2								
Saima	22	22	1.1–2.89	0.29–0.99	2.44–13.17	3.33–5.94	0.19–0.71	25.69–26.15	b.d.l.–0.24	0.06–0.13	2.77–3.08	0.43–0.87	0.11–0.78	1–2.2	13–116.3	39.2–58	39.2–58	Pilansberg	128	b.d.l.–2	1.14–4.81	5.37–12.05	4.38–7.73	0.08–2.48	23.56–25.83	0.08–1.12	b.d.l.–0.86	2.42–4.16	b.d.l.–1.93	0.58–b.d.l.(Fe)	b.d.l.–1.93	0.58–b.d.l.(Fe)	b.d.l.–1.93	0.58–b.d.l.(Fe)	b.d.l. = below detection limit.								
Kipawa	8	8	0.91–1.04	0.52–0.58	11.8–12.63	6.46–7.03	b.d.l.	25.92–26.08	b.d.l.–0.11	0.09–0.13	2.76–2.88	0.43–0.49	0.52–0.59	1.9–2	7.2–7.7	48.5–56.9	48.5–56.9	Norra Kärr	4	4	2.16–2.23	0.58–0.61	13.83–14.71	5.38–5.58	b.d.l.	26.07–26.2	0.02–0.03	0.04–0.05	2.61–2.74	0.32–0.34	0.27–0.28	3.9–4.9	57.2–86.4	61.2–65.1	61.2–65.1								

§: No. of EPMA analyses

*: No. of LA-ICP-MS analyses

Fe^{2+} in the $M(2)$ site, mostly in planar quadrangles (four-fold coordination), but with a small amount of Fe^{2+} in samples from Ilímaussaq and Tamazeght in square pyramids (five-fold coordination). Fe^{3+} occurs in distorted octahedral coordination with $\text{Fe}^{3+}/\Sigma\text{Fe}$ for the Ilímaussaq, Tamazeght and Mont Saint-Hilaire samples of 0.15(2), 0.09(2) and 0.07(2), respectively.

Trace elements

We present more than 400 LA-ICP-MS analyses of EGM from 69 samples from 12 occurrences (Figs 5, 6, Table 4). The HFSE are enriched to variable degrees by one to five orders of magnitude, but show no systematic correlation with textures or mineral assemblages. The *REE* are enriched by one to four orders of magnitude (relative to the primitive mantle of Palme and O'Neill, 2004; Fig. 5) and *REE* patterns vary in shape and degree of enrichment, allowing for a classification on the basis of (1) Eu anomalies and (2) light to heavy *REE* enrichment. Significant negative Eu anomalies are only found in EGM from occurrences where alkali basaltic parental melts are assumed or that are metamorphically overprinted (Ilímaussaq, Mont Saint-Hilaire, Ascension, Straumsvola (especially in EGM from the granite), Langesund, Kipawa and Norra Kärr). Negative Eu anomalies are absent in complexes where nephelinic parental melt compositions are assumed (Tamazeght, Lovozero, Khibiny, Saima and Poços de Caldas).

The relative enrichment of the *LREE* (La-Sm) compared to the *HREE* results in different shapes of the patterns. With respect to the *HREE* (Gd-Lu), the *LREE* (La-Sm) are more enriched in EGM from Ilímaussaq (Fig. 5a), Mont Saint-Hilaire (Fig. 5b), in the granite of Straumsvola (Fig. 5d) and Lovozero (Fig. 5g), displaying a mostly linear trend. EGM from Ascension (Fig. 5c) and Kipawa (Fig. 5k) have stronger enrichments of the *HREE* with a decrease (Ascension) or an increase (Kipawa) from Gd to Lu. EGM from nepheline syenites from Straumsvola (Fig. 5d) and Langesund (Fig. 5e) show continuously decreasing *LREE*, but increasing enrichment from Gd to Lu. Concave-shaped patterns are found in EGM from Tamazeght (Fig. 5h), Poços de Caldas (Fig. 5i) and in some EGM from Saima (Fig. 5j) and Khibiny (Fig. 5f), where the *LREE* are enriched to higher degrees than the *HREE*. Non-systematically varying *REE* distributions at different

localities are observed for EGM with comparable Mn/Fe ratios and concentration levels of Mn and Fe (compare, for example, EGM from Ascension and Tamazeght or Saima and Kipawa).

The LILE vary in a non-systematic zig-zag pattern and Ti, Cs, Rb, Be and B are generally enriched by up to two orders of magnitude. The strongest enrichment by three orders of magnitude for Ba is observed in EGM from Khibiny; whereas in EGM from Mont Saint-Hilaire, Ba can be enriched or slightly depleted by one order of magnitude in EGM of a single sample.

The compatible elements (V, Co, Ni, Cr) are invariably depleted or occur in concentrations below the detection limit. In contrast, Sc occurs at the ppm level and is invariably slightly enriched. Zn can be either enriched or depleted, and both trends may be seen in EGM from a single locality, e.g. at Mont Saint-Hilaire (Fig. 5b) and Khibiny (Fig. 5f).

P, Ti, Li and Cu invariably form negative spikes in EGM from all occurrences whereas Sr and Pb either show negative, positive or no anomalies at all; e.g. in EGM from Ilímaussaq, both negative and positive Pb anomalies are observed (Fig. 5a).

The Zr/Hf ratios of EGM from Ilímaussaq and Tamazeght correlate slightly positively with Mn/Fe (which we consider to be the most suitable monitor of fractionation, see discussion); whereas Zr/Hf remains constant with Mn/Fe in EGM from Mont Saint-Hilaire (Fig. 6a). Plotted vs. molar Mn/Fe, no systematic changes of the U/Th (Fig. 6b) and Nb/Ta (Fig. 6c) element ratios are observed for EGM from Ilímaussaq, Mont Saint-Hilaire and Tamazeght. EGM from all other occurrences have locality- or sample-specific constant Zr/Hf, U/Th and Nb/Ta ratios in common.

Discussion

Major and minor elements

Even after scrutinizing the full wealth of our mineral analyses and checking several possible fractionation indicators (such as Na/Ca), we find that the molar Mn/Fe ratio is the most important parameter to monitor fractionation in EGM (Johnsen and Gault, 1997; Pfaff *et al.*, 2008; Schilling *et al.*, 2009; Fig. 7a). Fe and Mn do not follow a strictly negative 1:1 correlation, not even within samples from a single locality, and the decrease of Fe and the increase of Mn occur to variable degrees (Figs 2, 3, 7). The maximum

TABLE 4. Trace elements in EGM.

	ppm	IIm	IIm	IIm	101_04	MSH	MSH	MSH	LHVMA5_EGM1	T612_EGM4	MSH	A _{Sc}	ST34_EGM2	Str	T38_EGM1	Str	L _{gs}
		1369_06	1335_20	101_04	52_EGM1	52_EGM3	52_EGM1	52_EGM3	LHVMA5_EGM1	T612_EGM4	H30(1)129	ST34_EGM2	ST34_EGM2	T38_EGM1	T38_EGM1	T38_EGM1	LGS_02
Tl	n.a.	n.a.	n.a.	n.a.	0.27	0.20	0.45	0.38	0.12	0.39	2.87	n.a.	n.a.	n.a.	n.a.	n.a.	n.a.
Cs	n.a.	n.a.	n.a.	n.a.	0.67	0.63	6.89	1.36	2.57	1.76	2.99	n.a.	n.a.	n.a.	n.a.	n.a.	n.a.
Rb	10.3	6.8	35.0	17.3	13.5	26.4	14.0	43.3	15.3	35.0	35.0	18.8	n.a.	n.a.	n.a.	n.a.	n.a.
Ba	1464	356	460	19.3	1.23	73.0	1124	73.1	186	310	310	146	n.a.	n.a.	n.a.	n.a.	n.a.
Be	n.a.	n.a.	n.a.	0.45	0.31	0.30	0.43	2.09	1.13	1.06	1.06	n.a.	n.a.	n.a.	n.a.	n.a.	n.a.
B	n.a.	n.a.	n.a.	2.20	0.85	5.68	6.02	6.54	6.32	3.11	3.11	n.a.	n.a.	n.a.	n.a.	n.a.	n.a.
Th	16.5	19.3	17.7	76.3	29.7	384	95.5	269	41.5	52.1	52.1	448	n.a.	n.a.	n.a.	n.a.	n.a.
U	22.8	46.7	42.1	16.3	34.2	213	423	51.4	47.2	152	152	44.4	n.a.	n.a.	n.a.	n.a.	n.a.
Nb	7952	6978	4925	26313	18309	16214	8139	11783	8085	28138	28138	18828	n.a.	n.a.	n.a.	n.a.	n.a.
Ta	709	530	304	5079	3646	163	257	816	1250	2841	2841	1241	n.a.	n.a.	n.a.	n.a.	n.a.
La	5564	4667	3936	23829	10153	20955	1468	7156	2085	17776	17776	12114	n.a.	n.a.	n.a.	n.a.	n.a.
Ce	9805	8007	7383	30526	13176	35913	1393	17365	3724	29292	29292	13773	n.a.	n.a.	n.a.	n.a.	n.a.
Pb	97.8	94.1	116	164	72.3	54.2	105	272	224	568	568	534	n.a.	n.a.	n.a.	n.a.	n.a.
Pr	1036	874	842	2508	1117	4104	89.6	2510	351	3066	3066	942	n.a.	n.a.	n.a.	n.a.	n.a.
Sr	1181	616	564	1239	151	772	3194	81.8	3611	2343	2343	2916	n.a.	n.a.	n.a.	n.a.	n.a.
Nd	3916	3311	3301	7025	2999	12789	203	12244	1071	10960	10960	1916	n.a.	n.a.	n.a.	n.a.	n.a.
Zr	94253	90734	102930	97472	87902	87370	90722	87260	87573	81394	81394	112797	n.a.	n.a.	n.a.	n.a.	n.a.
Hf	2542	2081	2108	2388	1608	1286	929	2009	1814	1670	1670	4485	n.a.	n.a.	n.a.	n.a.	n.a.
P	n.a.	n.a.	n.a.	n.a.	52.1	29.1	29.6	15.2	996	17.6	58.0	n.a.	n.a.	n.a.	n.a.	n.a.	n.a.
Sm	815	694	704	860	486	2325	29.9	4922	186	2121	2121	233	n.a.	n.a.	n.a.	n.a.	n.a.
Eu	86.6	69.4	71.5	68.6	39.2	186	3.51	459	40.8	114	114	26.3	n.a.	n.a.	n.a.	n.a.	n.a.
Ti	n.a.	n.a.	n.a.	n.a.	417	820	2177	3820	1446	1227	1227	n.a.	n.a.	n.a.	n.a.	n.a.	n.a.
Sn	n.a.	n.a.	n.a.	n.a.	35.1	32.6	16.6	247	107	45.3	128	n.a.	n.a.	n.a.	n.a.	n.a.	n.a.
Gd	742	644	693	683	462	1847	31.0	6623	195	1752	1752	167	n.a.	n.a.	n.a.	n.a.	n.a.
Dy	986	868	935	997	97.5	327	7.23	1386	41.3	264	264	37.6	n.a.	n.a.	n.a.	n.a.	n.a.
Li	n.a.	n.a.	n.a.	n.a.	5.04	5.00	5.94	3.33	33.1	33.1	33.1	3.62	n.a.	n.a.	n.a.	n.a.	n.a.
Y	4521	4153	4443	5115	4507	10181	685	34664	1756	9473	9473	2521	n.a.	n.a.	n.a.	n.a.	n.a.
Ho	213	191	207	220	183	435	16.6	2060	80.4	318	318	79.1	n.a.	n.a.	n.a.	n.a.	n.a.
Er	626	557	606	711	602	1248	66.3	5693	275	857	857	297	n.a.	n.a.	n.a.	n.a.	n.a.
Tm	96.1	87.5	95.2	125	101	192	13.7	717	47.8	112	112	56.5	n.a.	n.a.	n.a.	n.a.	n.a.
Yb	669	604	658	908	723	1174	121	3682	331	662	662	432	n.a.	n.a.	n.a.	n.a.	n.a.
Lu	104	94.8	104	120	97.5	137	19.9	416	44.1	84.6	84.6	69.9	n.a.	n.a.	n.a.	n.a.	n.a.
Cu	n.a.	n.a.	n.a.	n.a.	0.64	0.43	0.88	0.71	24.7	4.52	4.52	b.d.l.	n.a.	n.a.	n.a.	n.a.	n.a.
Sc	n.a.	n.a.	n.a.	n.a.	65.95	58.1	66.4	54.7	66.0	55.9	55.9	49.0	n.a.	n.a.	n.a.	n.a.	n.a.
V	n.a.	n.a.	n.a.	n.a.	b.d.l.	b.d.l.	0.05	5.30	0.18	0.18	0.18	0.18	n.a.	n.a.	n.a.	n.a.	n.a.

	Khib	Khib	Khib	Lov	Lov	PDC	PDC	Sm	KpW	NK
ppm	392-0_EGM2	KB-1_05	KB-1_05	LV02_07	364_EGM2	PDC_06	PDC_06	SM25_06	KpW_04	NK_EGM1
Co	n.a.	n.a.	n.a.	0.29	0.06	0.26	0.12	0.89	0.65	0.23
Ni	n.a.	n.a.	n.a.	b.d.l.	b.d.l.	b.d.l.	b.d.l.	1.68	b.d.l.	n.a.
Cr	n.a.	n.a.	n.a.	b.d.l.	b.d.l.	b.d.l.	b.d.l.	1.49	b.d.l.	n.a.
Zn	n.a.	n.a.	210	65.0	52.6	45.0	147	55.3	684	n.a.
Tl	0.20	n.a.	n.a.	n.a.	0.02	n.a.	n.a.	n.a.	n.a.	1.44
Cs	0.49	n.a.	n.a.	n.a.	2.22	n.a.	n.a.	n.a.	n.a.	7.13
Rb	14.4	24.0	1129	10.3	13.0	37.4	12.2	41.6	n.a.	37.6
Ba	2120	n.a.	n.a.	309	91.0	162	159	1821	1588	1.94
Be	1.30	n.a.	n.a.	n.a.	0.45	n.a.	n.a.	n.a.	n.a.	2.84
B	2.84	n.a.	n.a.	n.a.	2.53	n.a.	n.a.	n.a.	n.a.	42.5
Th	42.5	17.0	22.5	22.5	45.2	22.3	46.7	29.4	22.7	3.24
U	20.5	30.9	33.4	38.30	34.6	1027	59.1	59.1	29.4	13.3
Nb	13561	1030	5906	4752	5607	4942	5739	5739	896	896
Ta	647	114	541	453	142	42.5	765	765	15.7	15.7
La	6895	366	3663	2381	1663	7672	3682	3682	953	953
Ce	7924	760	7123	4664	1767	14362	6067	6067	1816	1816
Pb	162	9.21	40.1	57.5	35.4	99.7	116	116	52.2	52.2
Pr	601	88.3	829	581	113	1543	698	698	213	213
Sr	14145	10724	10328	5960	24344	28403	1466	1466	623	623
Nd	1648	392	2751	2534	296	5730	2461	2461	944	944
Zr	91668	95522	102803	103045	117226	105398	108726	108726	93843	93843
Hf	1785	1672	2249	2071	2185	18.8	1482	1482	1.482	1.482
P	59.5	n.a.	n.a.	14.1	n.a.	n.a.	n.a.	n.a.	n.a.	12.5
Sm	215	109	494	767	41.9	1169	823	823	303	303
Eu	60.2	39.3	140	239	13.0	311	116	116	40.4	40.4
Ti	2154	n.a.	n.a.	4140	n.a.	n.a.	n.a.	n.a.	1223	1223
Sn	33.8	n.a.	n.a.	19.9	n.a.	n.a.	n.a.	n.a.	121	121
Gd	215	132	431	759	36.5	873	1308	1308	399	399
Tb	41.5	27.3	75.0	128	7.94	122	348	348	83.6	83.6
Dy	346	188	504	805	59.7	62.6	3855	3855	650	650
Li	b.d.l.	n.a.	n.a.	1.12	n.a.	n.a.	n.a.	n.a.	b.d.l.	b.d.l.
Y	2403	1091	2773	3889	447	3669	26079	26079	6380	6380
Ho	83.4	43.0	106	157	15.0	100	1079	1079	153	153
Er	296	126	300	436	52.2	241	3995	3995	517	517
Tm	50.9	19.6	43.9	61.9	9.34	31.0	679	679	94.7	94.7
Yb	368	132	285	387	74.1	192	4509	4509	733	733
Lu	51.1	20.9	42.8	49.2	10.8	20.5	554	554	112	112
Cu	0.63	n.a.	n.a.	0.68	n.a.	n.a.	n.a.	n.a.	0.62	0.62

TABLE 4 (*contd.*).

ppm	Khib 392-0_EGM2	Khib KB-1.05	Lov LV02_07	Lov 364_EGM2	PDC PDC 06	Sm SM25_06	KPW KPW 04	NK NK_EGM1
Sc	60.6	n.a.	n.a.	65.6	n.a.	n.a.	n.a.	68.0
V	0.85	n.a.	n.a.	0.98	n.a.	n.a.	n.a.	0.28
Co	0.24	n.a.	n.a.	0.28	n.a.	n.a.	n.a.	0.31
Ni	b.d.l.	n.a.	n.a.	b.d.l.	n.a.	n.a.	n.a.	b.d.l.
Cr	1.97	n.a.	n.a.	b.d.l.	n.a.	n.a.	n.a.	0.14
Zn	83.0	n.a.	n.a.	36.6	n.a.	n.a.	n.a.	68.1

b.d.l. = below detection limit; n.a. = not analysed; other abbreviations as in Table 2.

EGM from alkali basaltic parental melts

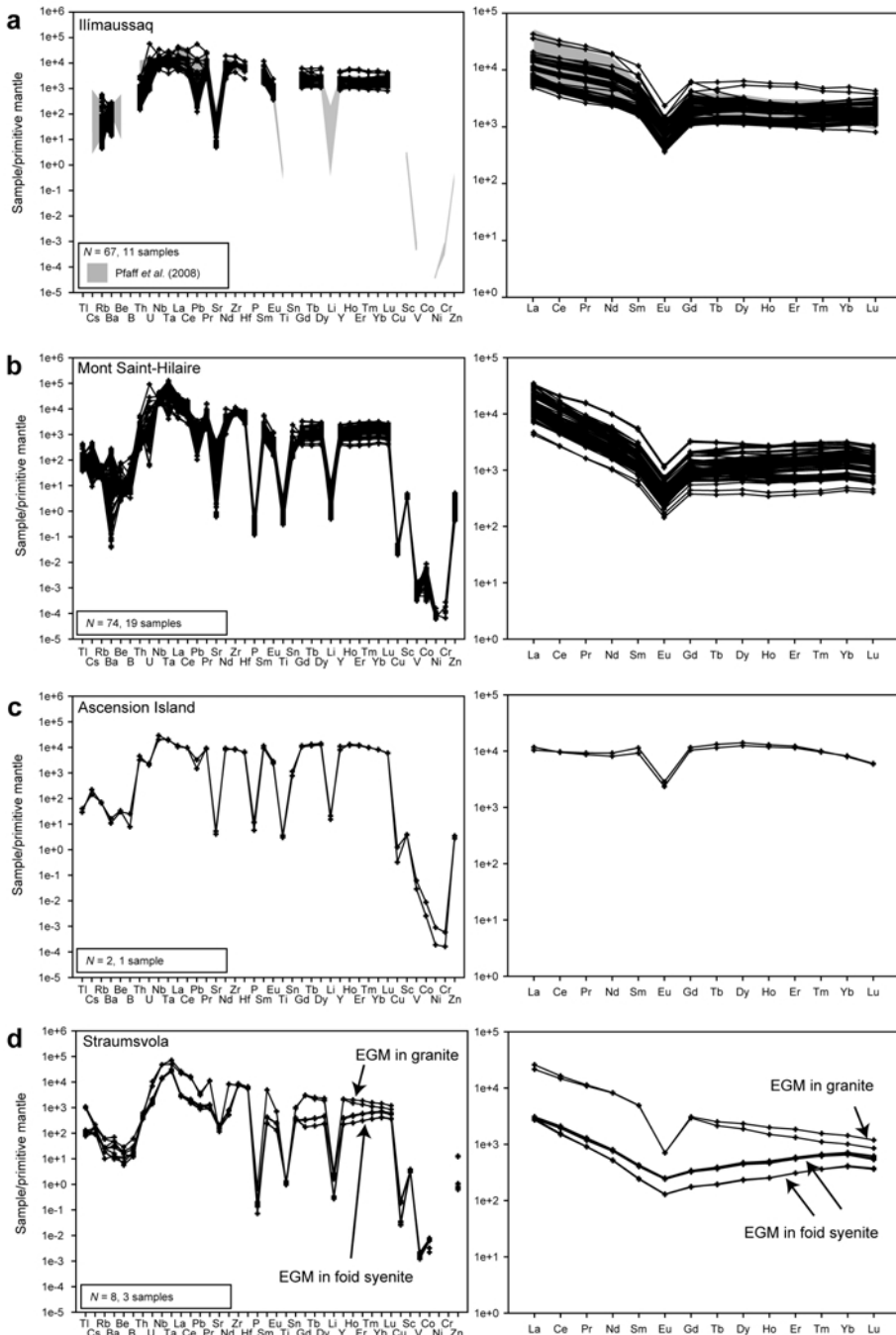
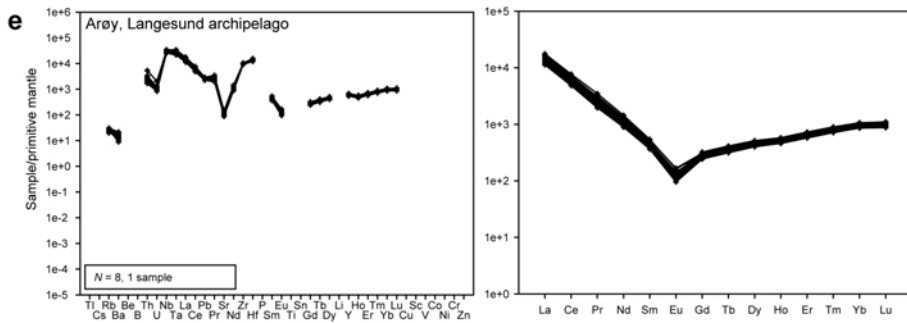
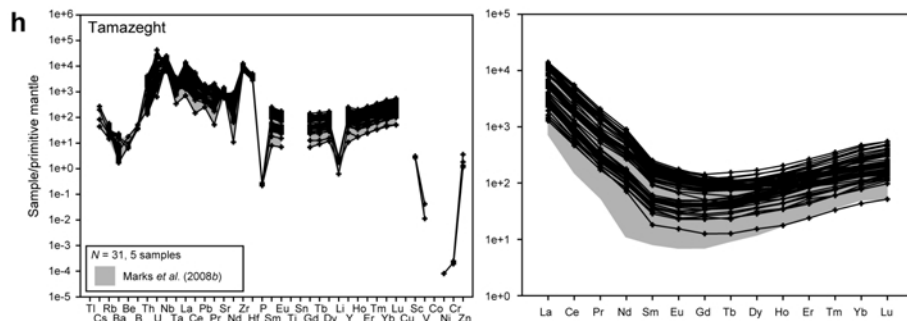
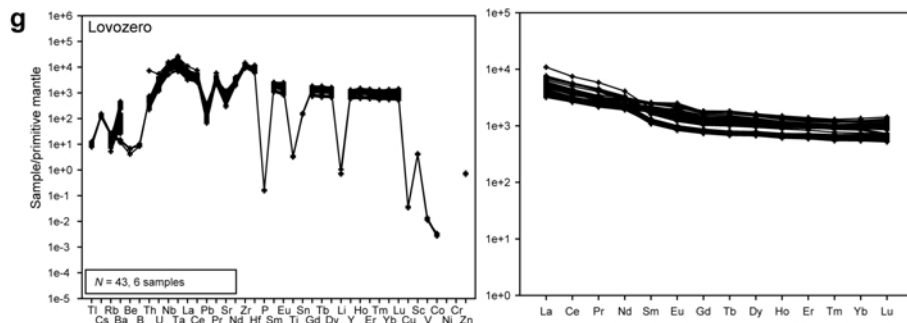
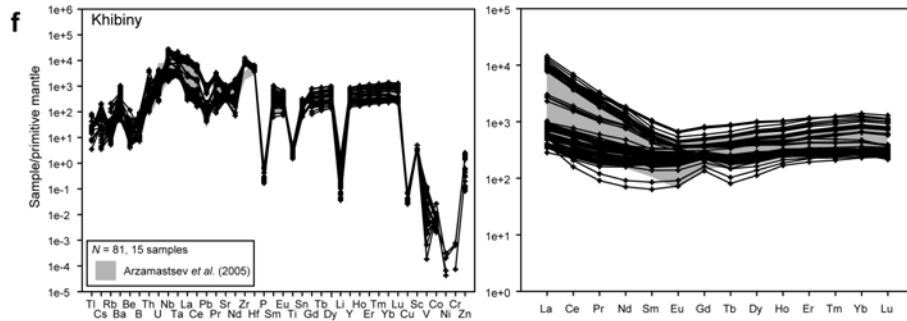


FIG. 5. Normalized trace elements and REE of EGM from the investigated occurrences. (a–e, above) Trace-element distributions of EGM from alkali basaltic parental melts; (f–j, next page) trace-element distributions of EGM from nephelinitic parental melts; (k–l, following page) trace-element distributions of EGM from metamorphosed complexes.

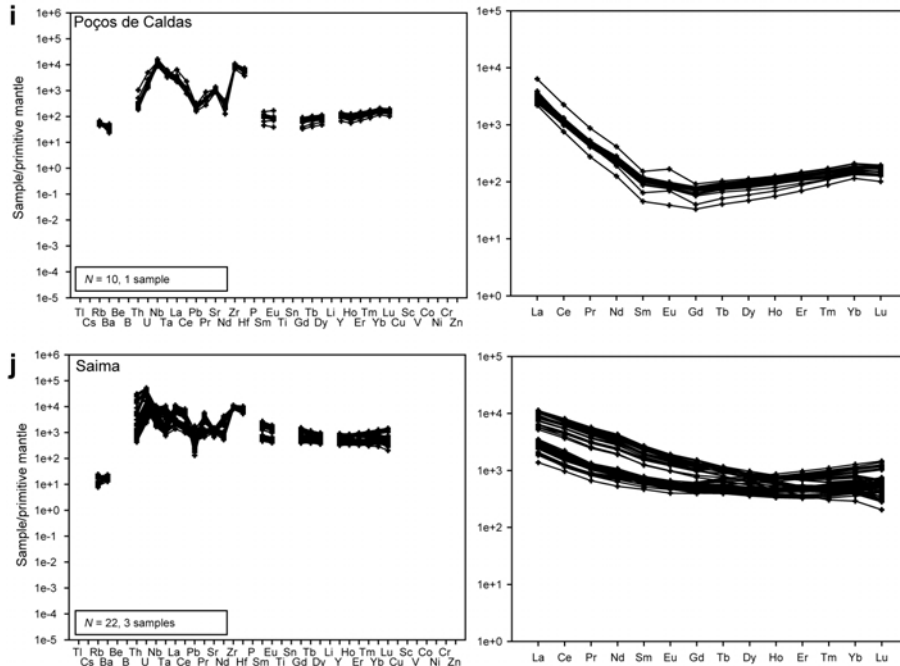
EGM from alkali basaltic parental melts



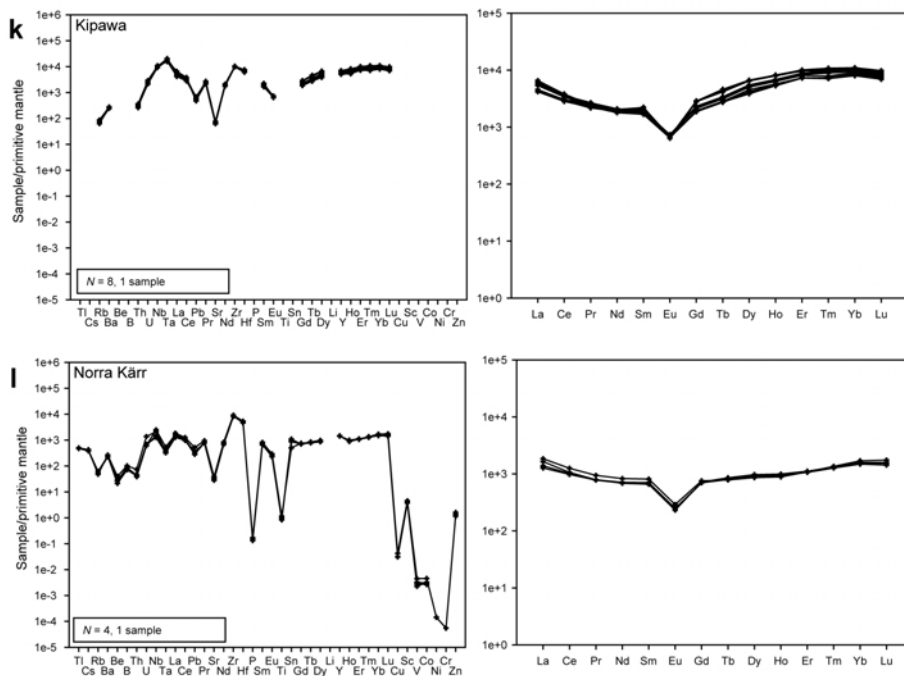
EGM from nephelinitic parental melts



EGM from nephelinitic parental melts



EGM from metamorphic rocks



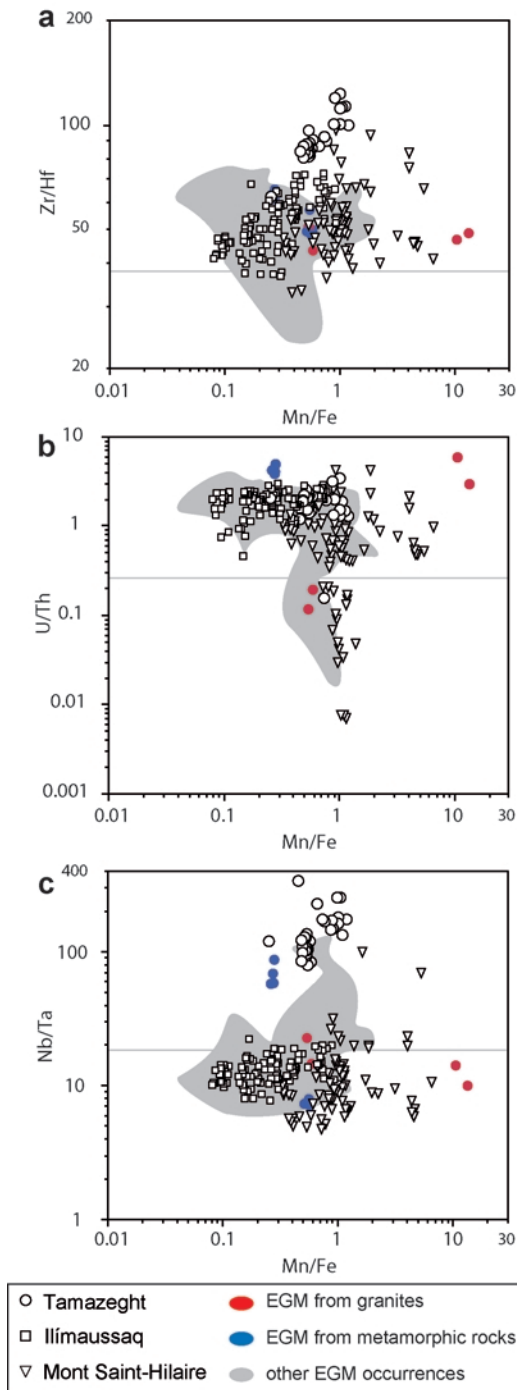


FIG. 6. Element ratios of the geochemical twins vs. Mn/Fe; (a) Zr/Hf; (b) U/Th; (c) Nb/Ta. Grey lines represent chondritic values.

amount of Mn found in any EGM is greater than the maximum Fe content, implying that Mn is preferred relative to Fe on the N-site (Rastsvetaeva, 2007). Three processes may control the incorporation of Fe and Mn into EGM: (1) the composition of the melt and its concentration levels of Fe and Mn; (2) the partition coefficients of Fe and Mn for eudialyte-melt that are probably temperature- and melt-composition dependent; and (3) co-crystallizing phases that favour one element over the other.

The exact Mn/Fe ratio of the melt at the time of EGM crystallization cannot be reconstructed, as most textures involving EGM display cumulate textures and thus, whole-rock data do not represent liquids. Although the Mn/Fe ratio of both melt and EGM increase with fractionation, the Mn/Fe ratios of EGM from Ilímaussaq are in contrast to (molar) whole rock data of Larsen and Steenfelt (1974, not shown), which were used by these authors to perform crystallization experiments and are believed to closely resemble melt compositions. Best-fit lines representing the (molar) Mn vs. Fe whole-rock data from Ilímaussaq have a different slope than best-fit lines representing the Fe and Mn (a.p.f.u.) distributions of EGM from this occurrence. Different EGM samples deviate non-systematically from the whole-rock data, which may indicate that, apart from temperature- and melt composition-dependent partition coefficients, EGM do not simply inherit the Mn/Fe ratio of the melt and that other minerals may discriminate in the incorporation between Fe and Mn. Hence, we interpret the Mn/Fe ratio of EGM to be mostly a function of the melt composition, but to be superimposed by crystal-chemical effects and by the availability of Mn and Fe, which, in turn, is controlled by co-crystallizing phases that incorporate Mn and Fe. In this regard, the most common Mn and Fe-incorporating minerals coexisting with EGM, clinopyroxene and amphibole, either do not influence or influence to an equal extent Mn/Fe in EGM (see below and Fig. 7e), but locally co-crystallizing minerals such as astrophyllite-group minerals may affect the Mn and Fe uptake into EGM.

EGM from nephelinitic parental magmas span the entire Mn and Fe ranges found and closely follow the negative 1:1 correlation line; whereas EGM from alkali basaltic parental melts show larger deviations from the negative 1:1 correlation line (Fig. 7b). EGM from metamorphosed complexes have small Mn (≤ 0.61 a.p.f.u.) but

COMPOSITIONAL VARIABILITY OF EUDIALYTE-GROUP MINERALS

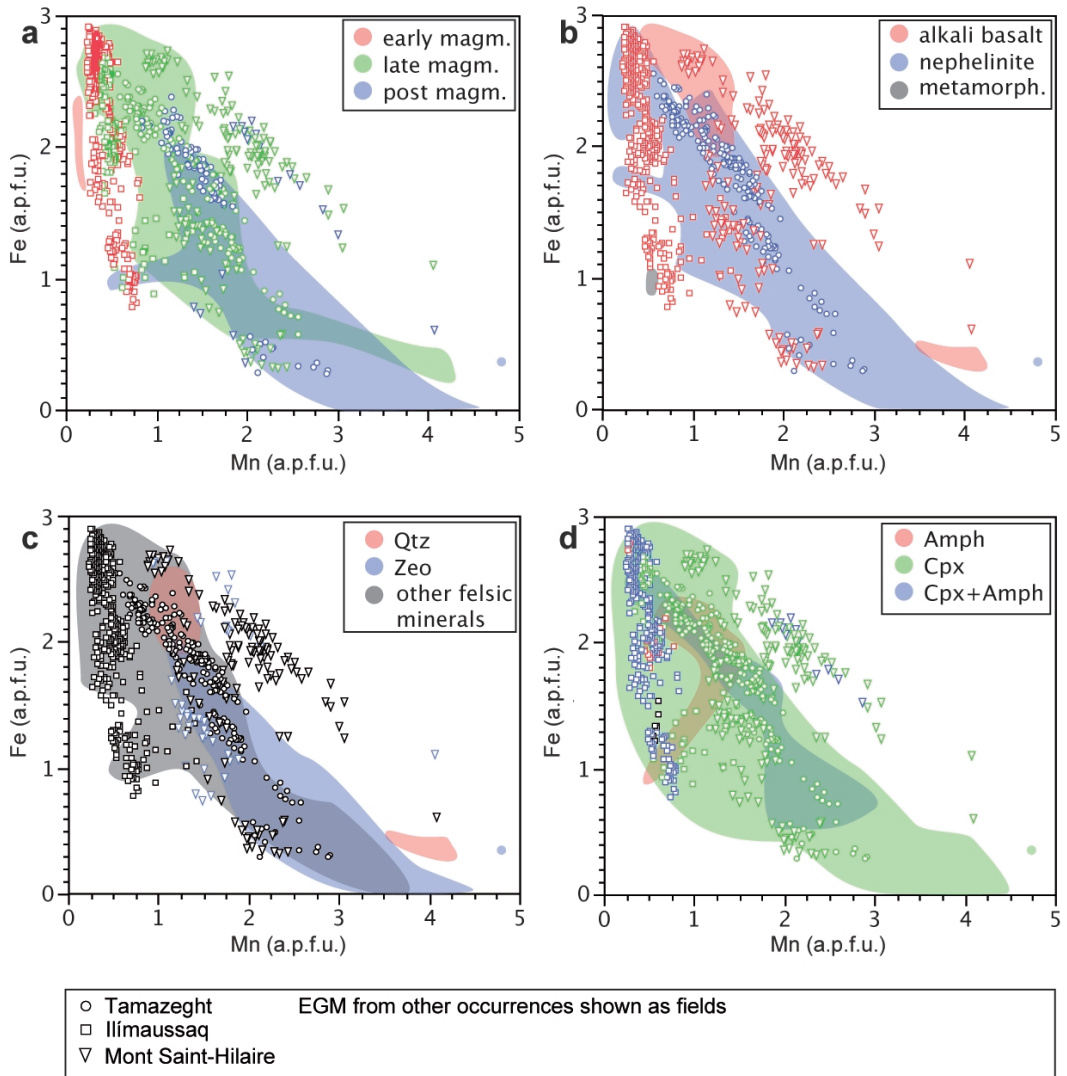


FIG. 7. Molar Mn vs. Fe in EGM: (a) colour-coded according to crystallization stage based on textural evidence and co-genetic minerals; (b) colour-coded according to parental melt or metamorphic overprint; (c) colour-coded according to assemblages with major felsic minerals; (d) colour-coded according to assemblages with major Fe-Mg silicates.

variable Fe contents (Fig. 7b). The presence of quartz in EGM-bearing assemblages does not affect the incorporation of Fe and Mn into EGM as both Fe-rich/Mn-poor (Ascension) and Fe-poor/Mn-rich (Straumsvola) EGM are observed to coexist in granites (Fig. 7c). EGM from late-stage assemblages at Pilansberg and Mont Saint-Hilaire coexist locally with zeolites

and are characterized by Mn contents >1 a.p.f.u. (Fig. 7c). The presence or absence of the Fe-Mg-silicates clinopyroxene and amphibole is not a prerequisite for the crystallization of EGM, but most EGM co-existing with amphibole are characterized by <1 a.p.f.u. Mn (Fig. 7d); thus, amphibole is more common in less evolved agpaitic rocks. Our dataset also confirms the

experimental results of Christophe-Michel-Lévy (1961) which suggested, at least in hydrothermal environments (e.g. from Pilansberg; Mitchell and Liferovich, 2006), that Fe-free EGM may form, while Mn-free EGM never do. We interpret the observation of nearly Fe-free EGM to support the idea that crystal-chemical effects co-control the incorporation of Mn and Fe into EGM.

Crystal chemistry of Fe in EGM

Observation of the most oxidized EGM analysed in this study, ILM 101, a late-magmatic sample from the Ilímaussaq complex, is in contrast to the reduced conditions determined in the Ilímaussaq lithologies. In fact, the most reduced conditions of any peralkaline rock system were found in Ilímaussaq (the augite syenite unit predating the agpaitic units: $\Delta\text{FMQ} = -2$ to -5 , Marks and Markl, 2001; see also Markl *et al.*, 2001). While some minerals reflect the $\text{Fe}^{3+}/\Sigma\text{Fe}$ and hence the oxygen fugacity of the coexisting melt (e.g. amphibole: King *et al.*, 2000), EGM cannot be used to monitor changes in the oxygen fugacity of the coexisting melt or fluid and other processes govern $\text{Fe}^{3+}/\Sigma\text{Fe}$ in EGM. Previous Mössbauer spectroscopy studies indicate that the $\text{Fe}^{3+}/\Sigma\text{Fe}$ of all natural eudialyses reported in the literature is <0.2 , except for those that are significantly hydrated (>5 wt.% H_2O : Pol'shin *et al.*, 1991; Khomyakov *et al.*, 2010). There is a roughly linear correlation between H concentration and $\text{Fe}^{3+}/\Sigma\text{Fe}$ in data compiled from the two papers above.

Eudialyte may be resistant to oxidation in certain environments (e.g. dry) due to the greater stability of Fe^{2+} in the four-fold $M(2)$ site relative to Fe^{3+} . Partially hydrated samples have greater $\text{Fe}^{3+}/\Sigma\text{Fe}$, but with Fe^{3+} in either five- or six-fold coordination, where the coordination of the planar quadrangle is increased by the addition of hydroxyl groups and/or water molecules (Khomyakov *et al.*, 2010). When sufficient oxygen is available (such as during heating of EGM in air), $\text{Fe}^{3+}/\Sigma\text{Fe}$ increases to 1 with all Fe^{3+} in either five- or six-fold coordination, where one to two O^{2-} anions are added to the planar quadrangle (Khomyakov *et al.*, 2010).

Based on the above, we suggest that the $\text{Fe}^{3+}/\Sigma\text{Fe}$ of natural EGM does not reflect primarily the oxygen fugacity, but rather the degree of hydration. We therefore infer that the Ilímaussaq sample was last equilibrated in more hydrous conditions compared to the Tamazeght and Mont Saint-Hilaire samples (see Pfaff *et al.*,

2008 and compare analyses presented by Pfaff *et al.*, 2010). As Mössbauer analyses were made over a length scale of roughly 1 mm, variations on smaller scales are averaged, which might explain why few EPMA analyses of ILM 101 reveal totals close to 100, even though Mössbauer spectroscopy indicates relatively high degrees of hydration.

Trace elements

The enrichment in LILE and HFSE and the depletion of the compatible elements are in accordance with the highly evolved character of the melts and/or fluids from which EGM were precipitated and we found Eu to correlate systematically with the apparent composition of the parental melt. Negative Eu anomalies are restricted to EGM from alkali basaltic parental melts, which experienced early plagioclase fractionation (e.g. Ilímaussaq: Bridgewater and Harry, 1968; Mont Saint-Hilaire: Greenwood and Edgar, 1984) and to metamorphic EGM localities. In contrast, EGM that crystallized from nephelinic parental melts and probably did not fractionate significant amounts of plagioclase have no negative Eu anomalies (e.g. Khibiny, Lovozero: Kramm and Kogarko, 1994; Tamazeght: Marks *et al.*, 2008b). This is consistent with the distinction of high-Ca agpaites from Ca-depleted agpaites as discussed in detail by Marks *et al.* (2011).

In Fig. 8, two groups of EGM are distinguished based on Eu/Eu^* : in the first group, EGM from nephelinic parental melts cluster around Eu/Eu^* values of 1 and hence are characterized by the absence of a Eu anomaly. The second group includes EGM from alkali basaltic parental melts and is characterized by Eu/Eu^* values ≤ 0.4 and thus shows a significant negative Eu anomaly. The relative enrichment of the LREE (Fig. 8a) and the HREE (Fig. 8b), and thus the general shape of the pattern, does not correlate with Eu/Eu^* and no further subdivision can be made. An alternative explanation for the lack of a Eu anomaly could be that the oxygen fugacity was too high to stabilize Eu^{2+} , although this is unlikely as agpaites generally form under reduced conditions (Ryabchikov and Kogarko, 2006; Markl *et al.*, 2010 and references given therein). We note that negative Eu anomalies coincide with negative spikes for Sr and Pb, but, on the other hand, negative anomalies of Sr and Pb do not necessarily arise together with Eu anomalies (Fig. 8c,d). Sr is strongly compatible in

COMPOSITIONAL VARIABILITY OF EUDIALYTE-GROUP MINERALS

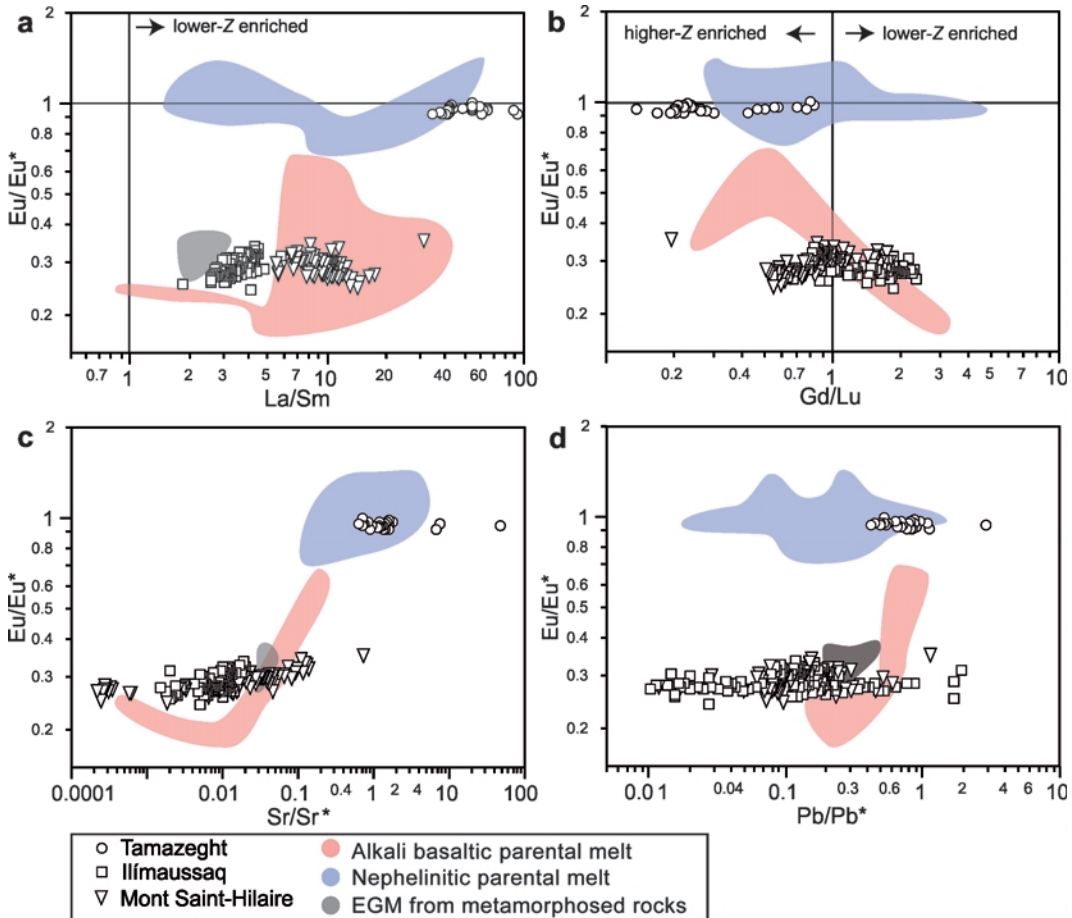


FIG. 8. (a) Relative enrichment of the LREE (La/Sm) vs. Eu/Eu^* . (b) Relative enrichment of the HREE (Gd/Lu) vs. Eu/Eu^* , where no systematic variations are observed for the Eu anomaly with the relative enrichment of increasing Z (Z = atomic number). (c) Sr/Sr^* vs. Eu anomaly showing a positive correlation. (d) Pb/Pb^* vs. Eu/Eu^* showing no correlation. EGM from Ilímaussaq, Mont Saint-Hilaire and Tamazeght are represented by distinct symbols, EGM from other occurrences are shown as fields: red represents EGM from alkali basaltic parental melts, blue represents EGM from nephelinitic parental melts and grey stands for EGM from metamorphosed host rocks.

plagioclase of any composition (e.g. Blundy and Wood, 1991; Bindemann *et al.*, 1998), while Ba, of which negative anomalies only correlate locally with Eu anomalies, is compatible only in Ab-rich plagioclase compositions (Bindemann *et al.*, 1998). These observations of Eu, Sr and Ba imply that plagioclase fractionation occurs to variable degrees and that compositionally heterogeneous plagioclase fractionates from melts which, at more evolved stages, crystallize EGM. Both plagioclase and ubiquitous alkali feldspar represent sinks for Pb, at least in more silicic

systems (e.g. Ewart and Griffin, 1994), which may explain non-systematic Pb variations in EGM. However, we cannot rule out the possibility that crustal contamination affects Sr/Sr^* and Pb/Pb^* (Marks *et al.*, 2004b). Negative Eu anomalies found in metamorphic EGM from Norra Kärr and Kipawa might be caused by metamorphic fluids in equilibrium with plagioclase-bearing lithologies, or represent the remnant of plagioclase fractionation of the parental melts. The latter melt composition would then have been alkali basaltic in both localities.

Pfaff *et al.* (2008) suggested that the crystallization of EGM potentially increases the Zr/Hf ratio of the melt and Marks *et al.* (2008b) showed that the crystallization of titanite, and to a lesser extent of zircon and EGM, modify the ratios of the geochemical twins (U/Th, Nb/Ta, Zr/Hf). Constant or sample-specific distinct Zr/Hf ratios plotted vs. Mn/Fe of most EGM imply that the net effect of EGM crystallization on the Zr and Hf budget of the melt is minor compared to the crystallization of other HFSE-incorporating minerals (Fig. 6). This becomes obvious when comparing the mineralogy of the agpaites from the kakortokites of Ilímaussaq and the foid-syenites from Tamazeght relative to the agpaites from Mont Saint-Hilaire. In the first two localities, EGM are the major sink of Zr and Hf (among other HFSE) due to their large modal abundances, and hence proceeding EGM crystallization is likely to control the Zr/Hf ratio of the evolving melt. At Mont Saint-Hilaire and most other occurrences, EGM are volumetrically subordinate HFSE-incorporating phases and thus may have a minor effect on the Zr and Hf budget of the melt.

EGM from various localities share negative anomalies for P, Li, Ti and Cu. These elements are effectively removed by the fractionation of apatite (P), amphibole (Li), Fe-Ti oxides, Ti-rich garnet, amphibole (Ti) and sulphides (Cu). These minerals typically occur as major or accessory phases in more primitive rock units of alkaline-peralkaline complexes (e.g. Marks and Markl, 2001; Marks *et al.*, 2004a; Ryabchikov and Kogarko, 2006; Pekov and Agakhanov, 2008; Schilling *et al.*, 2011). However, crystal-chemical effects play a secondary role in terms of trace element incorporation, because Sc, which is compatible in ubiquitous clinopyroxene (Marks *et al.*, 2004b), would be expected to be depleted in EGM, but instead it is invariably slightly enriched.

Variation of trace elements may be controlled by (1) the composition of the melt/fluid parental to EGM, (2) by previously crystallized or co-crystallizing phases, or by (3) crystal-chemical effects. In this respect, incorporation of different trace elements may be governed by any combination of the above factors and we cannot rule out possible processes for the following reasons: (a) As was shown using Fe and Mn compositional variations, the composition of the parental fluid/melt may influence the trace element uptake into EGM; however melt/fluid composition cannot be the sole factor. (b) The net effect of previously or

contemporaneously crystallizing phases on the trace element budget and on U/Th, Nb/Ta and Zr/Hf ratios cannot be reconstructed, because some important phases (e.g. baddeleyite, zircon, titanite, REE-phosphates, Nb-Ta-phases, Fe-Ti oxides, olivine, augite etc.; see e.g. Sørensen, 1997; Marks *et al.*, 2008b) may not be present in EGM-bearing samples, although their previous crystallization affected the trace-element budget of the melt/fluid. In addition, peralkaline rocks are mineralogically among the most diverse magmatic systems (Sørensen, 1997) and the liquidus relations of many exotic phases are poorly understood (e.g. Marr and Wood, 1992) and studies on the effect of changes of intensive parameters on the incorporation of HFSE in EGM are lacking. (c) Studies exploring crystal-chemical effects on the incorporation of trace elements into EGM are lacking.

Summary and conclusions

Major, minor and trace-element data allow the following conclusions to be made on the compositional variability of EGM and the generation and fractionation of EGM-bearing rocks:

(1) Textures, mineral assemblages and the composition of co-crystallizing phases imply a variably evolved character of the melts that precipitate EGM and textures and compositions are closely related to each other: early magmatic EGM invariably have smaller Mn/Fe values compared to later EGM (Johnsen and Gault, 1997; Pfaff *et al.*, 2008; Schilling *et al.*, 2009). The compositional spread of early-magmatic EGM is low and the substitution of Fe by Mn becomes more important with increasing degree of fractionation. The Mn/Fe ratio of EGM is controlled by the following processes: first by the fractionation stage and composition of the coexisting melt, second by crystal-chemical effects (the temperature- and melt composition-dependent Kd values for Mn and Fe), and third by co-crystallizing minerals. The latter point implies that, to a certain degree, EGM incorporates what is left from the crystallization of previously crystallizing Mn- and Fe-incorporating minerals.

(2) Investigation of the valence state of Fe in EGM reveals Fe^{2+} to predominate over Fe^{3+} . $\text{Fe}^{3+}/\Sigma\text{Fe}$ is not controlled by the oxygen fugacity of the melt, but is a function of the hydration state of EGM and possibly reflects the most recent re-equilibration of EGM.

(3) Melts parental to EGM-bearing rocks are heterogeneous in composition, depending on the actual composition of the mantle domain that undergoes partial melting, the degree of partial melting, contamination processes and various fractionation processes. Negative Eu anomalies are restricted to EGM from alkali basaltic parental melts (e.g. Larsen and Sørensen, 1987); whereas EGM from nephelinites invariably lack negative Eu anomalies (Kramm and Kogarko, 1994). The fractionation of apatite, amphibole, Fe-Ti oxides and sulphides occur independently from plagioclase fractionation and causes negative anomalies of, P, Li, Ti and Cu.

(4) Silica content is not a controlling factor for the crystallization of EGM, as EGM from peralkaline granites are compositionally similar to EGM from feldspathoid-bearing syenites.

(5) EGM occur stably in metamorphosed rocks. Obviously, high-grade (up to amphibolite facies) metamorphic fluids do not destabilize EGM.

(6) Trace-element compositions are controlled by a combination of different processes: EGM inherit characteristics from their parental melts (or fluids), which in turn are controlled by source characteristics and fractionation of previously crystallizing phases. In addition, crystal chemical effects contribute to the trace-element incorporation into EGM.

Acknowledgements

Peter Tarassoff and László Horváth kindly provided sample material from their collections from Mont Saint-Hilaire, and Sebastian Staude and Olga Apukhtina kindly supplied sample material from the Kola Peninsula. The sample material from Straumsvola and Ascension was obtained courtesy of Chris Harris. Ruslan Liferovich and Roger Mitchell are thanked for providing a dataset from their publication on Pilansberg. McGill University is thanked for the collaboration and the sampling permission in the Gault Nature Reserve, Mont Saint-Hilaire. Financial support from the DFG (grant MA 2135/12-1) is gratefully acknowledged. Indra Gill-Kopp is thanked for the sample preparation. Comments by the reviewers P. Piilonen, T. Andersen, and the associate editor R. Mitchell substantially improved the quality of the manuscript.

References

- Adams, F.D. (1903) The Monteregean Hills – A Canadian Petrographical Province? *Journal of Geology*, **11**, 239–282.
- Adamson, O.J. (1944) The petrology of the Norra Kärr district. *Geologiska Foereningen i Stockholm Foerhandlingar*, **66**, 113–255.
- Allan, J.F. (1992) Geology and mineralization of the Kipawa Yttrium-Zirconium Prospect, Quebec. *Exploration and Mining Geology*, **1**, 283–295.
- Andersen, T., Erambert, M., Larsen, A.O. and Selbekk, R.S. (2010) Petrology of nepheline syenite pegmatites in the Oslo rift, Norway: Zirconium silicate mineral assemblages as indicators of alkalinity and volatile fugacity in mildly aphytic magma. *Journal of Petrology*, **51**, 2303–2325.
- Anthony, E.Y., Segalstad T.V. and Neumann, E.-R. (1989) An unusual mantle source region for nephelinites from the Oslo Rift, Norway. *Geochimica et Cosmochimica Acta*, **53**, 1067–1076.
- Arzamastsev, A.A., Bea, F., Arzamastseva, L.V. and Montero, P. (2002) Rare earth elements in rocks and minerals from alkaline plutons of the Kola Peninsula, NW Russia, as indicators of alkaline magma evolution. *Russian Journal of Earth Sciences*, **10**, 187–209.
- Arzamastsev, A.A., Bea, F., Arzamastseva, L.V. and Montero, P. (2005) Trace elements in minerals of the Khibiny Massif as indicators of mineral formation evolution: results of LA-ICP-MS study. *Geochemistry International*, **43**, 71–85.
- Bailey, J.C., Gwozdz, R., Rose-Hansen, J. and Sørensen, H. (2001) Geochemical overview of the Ilímaussaq alkaline complex, South Greenland. *Geology of Greenland Survey Bulletin*, **190**, 35–53.
- Bindemann, I.N., Davis, A.M. and Drake, M.J. (1998) Ion microprobe study of plagioclase-basalt partition experiments at natural concentration levels of trace elements. *Geochimica et Cosmochimica Acta*, **62**, 1175–1193.
- Blaxland, A.B. (1977) Aphytic magmatism at Norra Kärr? Rb-Sr isotopic evidence. *Lithos*, **10**, 1–8.
- Blundy, J.D. and Wood, B.J. (1991) Crystal-chemical controls on the partitioning of Ba and Sr between plagioclase feldspar, silicate melts and hydrothermal solutions. *Geochimica et Cosmochimica Acta*, **55**, 193–209.
- Bohse, H., Brooks, C.K. and Kunzendorf, H. (1971) Field observations on the kakortokites of the Ilímaussaq intrusion, South Greenland, including mapping and analyses by portable X-ray fluorescence equipment for zirconium and niobium. *Rapport Grønlands Geologiske Undersøgelse*, **38**, 43 pp.
- Bouabdli, A., Dupuy, C. and Dostal, J. (1988) Geochemistry of Mesozoic alkaline lamprophyres

- and related rocks from the Tamazert massif, High Atlas (Morocco). *Lithos*, **22**, 43–58.
- Bridgewater, D. and Harry, W.T. (1968) Anorthosite xenoliths and plagioclase megacrysts in Precambrian intrusions of South Greenland. *Meddelelser om Grönland*, **185**, 1–243.
- Brøgger, W.C. (1890) Die Mineralien der Syenitpegmatitgänge der südnorwegischen Augit- und Nephelinsyenite. *Zeitschrift für Kristallographie*, **16**, 1–63.
- Christophe-Michel-Lévy, M. (1961) Reproduction artificielle de quelques minéraux riches en zirconium (zircon, eudialyt, elpidite): Comparison avec leurs conditions naturelles de formation. *Bulletin de la Société française de Minéralogie*, **84**, 265–269.
- Coulson, I.A. (1997) Post-magmatic alteration in eudialyte from the North Qôroq centre, South Greenland. *Mineralogical Magazine*, **61**, 99–109.
- Coulson, I.A. and Chambers, A.D. (1996) Patterns of zonation in rare-earth-bearing minerals in nepheline syenites of the North Qôroq center, South Greenland. *The Canadian Mineralogist*, **34**, 1163–1178.
- Currie, K.L., Eby, G.N., and Gittins, F. (1986) The petrology of the Mont Saint-Hilaire complex, southern Quebec: An alkaline gabbro-peralkaline syenite association. *Lithos*, **19**, 65–81.
- Eby, G.N. (1985) Sr and Pb isotopes, U and Th chemistry of the alkaline Monteregian and White Mountain igneous provinces, eastern North America. *Geochimica et Cosmochimica Acta*, **49**, 1143–1153.
- Edgar, A.D. and Blackburn, C.E. (1972) Eudialyte from the Kipawa Lake area, Temiscamingue County, Quebec. *The Canadian Mineralogist*, **11**, 554–559.
- Ewart, A. and Griffin, W.L. (1994) Application of proton-microprobe data to trace-element partitioning in volcanic rocks. *Chemical Geology*, **117**, 251–284.
- Ferguson, J. (1964) Geology of the Ilímaussaq alkaline intrusion, South Greenland. Description of map and structure. *Bulletin Grønlands Geologiske Undersøgelse*, **39**, 1–82.
- Gerasimovskiy, V.I., Volkov, V.P., Kogarko, L.N., and Polyakov, A.I. (1974) Kola peninsula. Pp. 206–221 in: The alkaline rocks (H. Sørensen, editor). Wiley, London.
- Gold, D.P. (1967) Alkaline ultrabasic rocks in the Montreal area, Quebec. Pp. 288–302 in: *Ultramafic and Related Rocks* (P.J. Wyllie, editor). Wiley, New York.
- Greenwood, R.C. and Edgar, A.D. (1984) Petrogenesis of the gabbros from Mt St. Hilaire, Quebec, Canada. *Geological Journal*, **19**, 353–376.
- Griffin, W.L., Powell, W.J., Pearson, N.J. and O'Reilly, S.Y. (2008) GLITTER: Data reduction software for laser ablation ICP-MS (appendix). Pp 308–311 in: *Laser Ablation in the Earth Sciences* (P. Sylvester, editor). Mineralogical Association of Canada (MAC) Short Course Series Vol. **40**, Ottawa, Ontario, Canada.
- Harris, C. (1986) A quantitative study of magmatic inclusions in the plutonic ejecta of Ascension Island. *Journal of Petrology*, **27**, 251–276.
- Harris, C. and Rickard, R.S. (1987) Rare-earth-rich eudialyte and dalyte from a peralkaline granite dyke at Straumsvola, Dronning Maud Land, Antarctica. *The Canadian Mineralogist*, **25**, 755–762.
- Harris, C., Cressey, J.D., Bell, F.B., Atkins, F.B. and Beswetherick, S. (1982) An occurrence of rare-earth-rich eudialyte from Ascension Island, South Atlantic. *Mineralogical Magazine*, **46**, 421–425.
- Hettmann, K. (2009) *Der Randpegmatite der Ilímaussaq Intrusion, Südwest Grönland*. Diploma thesis, Universität Tübingen, Germany, 84 pp.
- Horváth, L. and Gault, R.A. (1990) The mineralogy of Mont Saint Hilaire, Quebec. *The Mineralogical Record*, **21**, 284–392.
- Jacob, D.E. (2006) High sensitivity analysis of trace element-poor geological reference glasses by Laser Ablation-Inductively Coupled Plasma-Mass Spectrometry (LA-ICP-MS). *Geostandards and Geoanalytical Research*, **30**, 221–235.
- Jochum, K.P. and Nohl, U. (2008) Reference materials in geochemistry and environmental research and the GeoReM database. *Chemical Geology*, **253**, 50–53.
- Johnsen, O. and Gault, R.A. (1997) Chemical variation in eudialyte. *Neues Jahrbuch für Mineralogie, Abhandlungen*, **171**, 215–237.
- Johnsen, O. and Grice, J.D. (1999) The crystal chemistry of the eudialyte group. *The Canadian Mineralogist*, **37**, 865–891.
- Johnsen, O., Ferraris, G., Gault, R.A., Grice, J.D., Kampf, A.R. and Pekov, I.V. (2003) The nomenclature of eudialyte-group minerals. *The Canadian Mineralogist*, **41**, 785–794.
- Kchit, A. (1990) *Le plutonisme alcalin du Tamazeght (Haut Atlas de Midelt, Maroc)*. Thèse 3e cycle, Université Paul Sabatier, Toulouse, France, 302 pp.
- Khomyakov, A.P., Korovushkin, V.V., Perfiliev, Y.D. and Cherepanov, V.M. (2010) Location, valence states, and oxidation mechanism of iron in eudialyte-group minerals from Mössbauer spectroscopy. *Physics and Chemistry of Minerals*, **37**, 543–554.
- King, P.L., Hervig, R.L., Holloway, J.S., Delaney, M.D. and Dyar, M.D. (2000) Partitioning of $\text{Fe}^{3+}/\text{Fe}_{\text{tot}}$ between amphibole and basanitic melt as a function of oxygen fugacity. *Earth and Planetary Science Letters*, **178**, 97–112.
- Kogarko, L.N., Lazutkina, L.N. and Romanchev, B.P. (1982) The origin of eudialyte mineralization. *Geochemistry International*, **19**, 128–145.
- Kogarko, L.N., Lahaye, Y. and Brey, G.P. (2010) Plume-related mantle source of super-large rare metal deposits from the Lovozero and Khibina

COMPOSITIONAL VARIABILITY OF EUDIALYTE-GROUP MINERALS

- massifs on the Kola Peninsula, Eastern part of Baltic Shield: Sr, Nd and Hf isotope systematics. *Mineralogy and Petrology*, **98**, 197–208.
- Kramm, U. and Kogarko, L.N. (1994) Nd and Sr isotope signatures of the Khibina and Lovozero agpaitic centres, Kola Alkaline Province, Russia. *Lithos*, **32**, 225–242.
- Larsen, A.O. (2010) *The Langesundfjord*. History, Geology, Pegmatites, Minerals. Bode Verlag, Salzhemmendorf, 239 pp.
- Larsen, L.M. and Sørensen, H. (1987) The Ilímaussaq intrusion – progressive crystallization and formation of layering in an agpaitic magma. Pp. 473–488 in: *Alkaline Igneous Rocks* (J.G. Fitton and B.G.J. Upton, editors). Blackwell, London.
- Larsen, L.M. and Steenfelt (1974) Alkali loss and retention in an iron-rich peralkaline phonolite dyke from the Garder province, South Greenland. *Lithos*, **7**, 81–90.
- Leat, P.T., Curtis, M.L., Riley, T.R. and Ferraccioli, F. (2007) Jurassic magmatism in Dronning Maud Land; results of the MAMOG project, in Antarctica: A Keystone in a Changing World. *Online Proceedings of the 10th ISAES*, edited by A.K. Cooper, C.R. Raymond et al. USGS Open-File Report, **2007-1047**, Short Research Paper 033, 4 pp.
- Lurie, J. (1986) Mineralization of the Pilanesberg Alkaline complex. Pp. 2215–2228 in: Mineral deposits of South Africa, 2 (C.R. Anhaeusser, and S. Maske, editors). The Geological Society of South Africa, Johannesburg.
- Lustrino, M., Dallai, L., Giordano, R., Gomes, C.B., Melluso, L., Morbidelli, L., Ruberti, E., and Tassinari, C.C.G. (2003) Geochemical and Sr-Nd-O isotopic features of the Poços de Caldas alkaline massif (Sp-Mg, SE Brazil): Relationships with the Serra do Mar analogues. *Short papers – IV. South American Symposium on Isotope Geology*, 593–595.
- Markl, G., Marks, M., Schwinn, G. and Sommer, H. (2001) Phase equilibrium constraints on intensive crystallization parameters of the Ilímaussaq Complex, South Greenland. *Journal of Petrology*, **42**, 2231–2258.
- Markl, G., Marks, M.A.W. and Frost, B.R. (2010) On the controls of oxygen fugacity in the generation and crystallization of peralkaline melts. *Journal of Petrology*, **51**, 1831–1847.
- Marks, M. and Markl, G. (2001) Fractionation and assimilation processes in the alkaline augite syenite unit of the Ilímaussaq intrusion, South Greenland as deduced from phase equilibria. *Journal of Petrology*, **42**, 1947–1969.
- Marks, M., Vennemann, T., Siebel, W. and Markl, G. (2004a) Nd-, O-, and H-isotopic evidence for complex, closed-system fluid evolution of the peralkaline Ilímaussaq intrusion, South Greenland. *Geochimica et Cosmochimica Acta*, **68**, 3379–3395.
- Marks, M., Halama, R., Wenzel, T. and Markl, G. (2004b) Trace element variations in clinopyroxene and amphibole from alkaline to peralkaline syenites and granites: implications for mineral-melt trace-element partitioning. *Chemical Geology*, **211**, 185–215.
- Marks, M.A.W., Schilling, J., Coulson, I.M., Wenzel, T. and Markl, G. (2008a) The alkaline-peralkaline Tamazeght complex, High Atlas Mountains, Morocco: Mineral chemistry and petrological constraints for derivation from a compositionally heterogeneous mantle source. *Journal of Petrology*, **46**, 1097–1131.
- Marks, M.A.W., Coulson, I.M., Schilling, J., Jacob, D.E., Schmitt, A.K. and Markl, G. (2008b) The effect of titanite and other HFSE-rich mineral (Ti-bearing andradite, zircon, eudialyte) fractionation on the geochemical evolution of silicate melts. *Chemical Geology*, **257**, 153–172.
- Marks, M.A.W., Hettmann, K., Schilling, J., Frost, B.R. and Markl, G. (2011) The mineralogical diversity of alkaline igneous rocks: critical factors for the transition from miaskitic to agpaitic phase assemblages. *Journal of Petrology*, **52**, 439–455.
- Marr, R.A. and Wood, S.A. (1992) Preliminary petrogenetic grids for sodium and calcium zirconosilicate minerals in felsic peralkaline rocks: The $\text{SiO}_2\text{-Na}_2\text{ZrO}_3$ and $\text{SiO}_2\text{-CaZrO}_3$ pseudobinary systems. *American Mineralogist*, **77**, 810–820.
- Mitchell, R.H. and Liferovich, R.P. (2006) Subsolidus deuterium/hydrothermal alteration of eudialyte in lujavrite from the Pilanesberg alkaline complex, South Africa. *Lithos*, **91**, 352–372.
- Olivo, G.R. and Williams-Jones, A.E. (1999) Hydrothermal REE-rich eudialyte from the Pilanesberg complex, South Africa. *The Canadian Mineralogist*, **37**, 653–663.
- Palme, H. and O'Neill, H.S.C. (2004) Cosmochemical estimates on mantle composition. Pp. 1–38 in: *Treatise on Geochemistry 2* (R.W. Carlson, editor). Elsevier, Amsterdam.
- Pekov, I.V. and Agakhanov, A.A. (2008) Thallium-rich murunskite from the Lovozero pluton, Kola Peninsula, and partitioning of alkali metals and thallium between sulfide minerals. *Geology of Ore Deposits*, **50**, 583–589.
- Pfaff, K., Krumrei, T., Marks, M., Wenzel, T., Rudolf, T. and Markl, G. (2008) Chemical and physical evolution of the lower layered sequence from the syenitic Ilímaussaq intrusion, South Greenland: Implications for the origin of magmatic layering in peralkaline felsic liquids. *Lithos*, **106**, 280–296.
- Pfaff, K., Wenzel, T., Schilling, J., Marks, M. and Markl, G. (2010) A fast and easy-to-use approach to cation site assignment for eudialyte-group minerals.

- Neues Jahrbuch für Mineralogie, Abhandlungen*, **187**, 69–81.
- Pol'shin, E.V., Platonov, A.N., Borutzky, B.E., Taran, M.N. and Rastsvetaeva, R.K. (1991) Optical and Mössbauer study of minerals of the eudialyte group. *Physics and Chemistry of Minerals*, **18**, 117–125.
- Rastsvetaeva, R.K. (2007) Structural mineralogy of the eudialyte group: A review. *Crystallography Reports*, **52**, 47–64.
- Roedder, E. and Coombs, D.S. (1967) Immiscibility in granitic melts, indicated by fluid inclusions in ejected granitic blocks from Ascension Island. *Journal of Petrology*, **8**, 417–451.
- Ryabchikov, I.D. and Kogarko, L.N. (2006) Magnetite compositions and oxygen fugacities of the Khibina magmatic system. *Lithos*, **91**, 35–45.
- Schilling, J., Marks, M., Wenzel, T. and Markl, G. (2009) Reconstruction of magmatic to subsolidus processes in an agpaitic system using eudialyte textures and composition: A case study from Tamazeght, Morocco. *The Canadian Mineralogist*, **47**, 351–365.
- Schilling, J., Frost, B.R., Marks, M.A.W., Wenzel, T. and Markl, G. (2011) Fe-Ti oxide-silicate (QUIIF-type) equilibria in feldspathoid-bearing systems. *American Mineralogist*, **96**, 100–110.
- Schollenbruch, K. (2007) *Spätmagmatische Eudialyt-führende Alkalifeldspat-syenite innerhalb der Kakortokit-Sequenz der Ilimaussaq-Intrusion, Südgrönland*. Diploma thesis, Universität Tübingen, Germany, 138 pp.
- Schönenberger, J. and Markl, G. (2008) The magmatic and fluid evolution of the Motzfeldt Intrusion in South Greenland: Insights into the formation of agpaitic and miaskitic rocks. *Journal of Petrology*, **49**, 1549–1577.
- Schorscher, H.D. and Shea, M.E. (1992) The regional geology of the Poços de Caldas alkaline complex: Mineralogy and geochemistry of selected nepheline syenites and phonolites. *Journal of Geochemical Exploration*, **45**, 25–51.
- Shand, S.I. (1928) The geology of Pilansberg in the Western Transvaal. Geological Society of South Africa. *Transactions*, **31**, 91–156.
- Sørensen, H. (1974) Kola peninsula. Pp. 206–221 in: *The Alkaline Rocks* (H. Sørensen, editor). Wiley, London.
- Sørensen, H. (1992) Agpaitic nepheline syenites: A potential source of rare minerals. *Applied Geochemistry*, **7**, 417–427.
- Sørensen, H. (1997) The agpaitic rocks – an overview. *Mineralogical Magazine*, **61**, 485–498.
- Stromeyer, F. (1819) Summary of meeting 16 December 1819. *Göttingische gelehrte Anzeigen*, **3**, 1993–2000.
- Törnebohm, A.E. (1906) Katapleit-syenit. *Sveriges Geologiska Undersökning, Ser. C*, **199**, 1–54.
- Ussing, N.V. (1912) Geology of the country around Julianehaab, Greenland. *Meddelelser om Grönland*, **38**, 376 pp.
- Wight, Q. and Chao, G. (1995) Mont Saint-Hilaire Revisited Part 2. *Rocks and Minerals*, **70**, 90–103; 131–138.
- Wu, F.-Y., Yang, Y.-H., Marks, M.A.W., Liu, Z.-C., Zhou, Q., Ge, W.-C., Yang, J.-S., Zhao, Z.-S., Mitchell, R.H. and Markl, G. (2010) In situ U-Pb, Nd and Hf isotopic analysis of eudialyte by LA-(MC)-ICP-MS. *Chemical Geology*, **273**, 8–34.

Appendix

LA-ICP-MS results for the BCR2G standard

GeoReM preferred values are from the <http://georem.mpch-mainz.gwdg.de/> homepage and from Jochum and Nohl (2008) and are given in ppm, except for P and Ti which are given in wt.%.

BCR2G	GeoReM preferred values (ppm)	Average (n = 20)	Standard deviation	Relative standard deviation
Tl	0.30	0.23	0.02	0.09
Cs	1.16	1.16	0.06	0.05
Rb	47	48.1	2.85	0.06
Ba	683	697	39.34	0.06
Be	2.30	2.30	0.21	0.09
B	6.00	6.91	2.20	0.32
Th	5.90	6.56	0.76	0.12
U	1.69	1.72	0.12	0.07
Nb	12.5	12.7	1.27	0.10
Ta	0.78	0.86	0.12	0.14
La	24.7	27.1	2.60	0.10
Ce	53.3	54.3	3.97	0.07
Pb	11.0	10.7	0.77	0.07
Pr	6.70	7.07	0.55	0.08
Sr	342	356	30.73	0.09
Nd	28.9	31.1	2.95	0.09
Zr	184	188	24.10	0.13
Hf	4.84	5.21	0.63	0.12
P ₂ O ₅ (wt.%)	0.37	0.34	0.02	0.05
Sm	6.59	7.15	0.69	0.10
Eu	1.97	2.09	0.18	0.09
TiO ₂ (wt.%)	2.27	2.65	0.21	0.08
Sn	2.60	3.99	1.39	0.35
Gd	6.71	7.22	0.74	0.10
Tb	1.02	1.09	0.13	0.12
Dy	6.44	7.11	0.89	0.12
Li	9.00	9.46	0.48	0.05
Y	35.0	36.9	4.48	0.12
Ho	1.27	1.42	0.18	0.12
Er	3.70	3.93	0.48	0.12
Tm	0.51	0.58	0.08	0.13
Yb	3.39	3.88	0.47	0.12
Lu	0.50	0.58	0.07	0.12
Cu	21.0	17.3	1.31	0.08
Sc	33.0	38.3	3.99	0.10
V	425	436	25.80	0.06
Co	38.0	38.0	1.94	0.05
Ni	13.0	12.4	0.79	0.06
Cr	17.0	17.1	1.17	0.07
Zn	125	143	9.72	0.07

